THE

EVALUATION

OF

SAILING VEHICLE RIG POLARS

FROM

TWO-DIMENSIONAL WIND TUNNEL DATA

by

W. S. Bradfield and Lee M. Griswold

State University of New York

College of Engineering and Applied Science

Department of Mechanical Engineering

Report No. 285

January 1977

Nomenclature

a = wave amplitude (trough to crest)

A = area

$A\!R$ = geometric aspect ratio = $[(span)^2/area]$

c = sail chord

C = coefficient = $[force/\frac{1}{2}\rho V^2 A]$

C_H = heeling force coefficient; perpendicular to thrust line (see Figure 2)

C_{R_a} = aerodynamic resultant force coefficient; $C_{R_a} = \sqrt{C_C^2 + C_D^2}$

Da = aerodynamic drag force; parallel to apparent wind vector $(\vec{V}_a)$; $D_a = D_i + D_\pi + d$

D_h = hydrodynamic drag force; parallel to boat velocity vector (V_b)

h = sail maximum camber

LWL = load waterline length

$\vec{R}$ = resultant force vector

R_c = Vc/ν

T = thrust $(C_T = T/\frac{1}{2}\rho V_a^2 A)$

$\vec{V}$ = velocity vector, speed and direction

V = speed

W = all up weight, pounds (including foils and crew)

z = height above sea level

α = angle of attack of foil

β = apparent wind angle

δ_a = aerodynamic drag angle, $\delta_a = \sin^{-1}[Da/Ra]$

λ = leeway angle

Φ = heel angle

ν = kinematic viscosity

π = parasite

ρ = density

τ = true wind angle

Subscripts

a = aerodynamic or apparent

b = boat

c = crosswind

d = sail section (two-dimensional) drag

f = friction

h = hydrodynamic

i = induced (drag)

s = sail

τ = true wind angle

$\rightarrow$ = vector quantity giving both magnitude and direction

PART 1

Introduction

As sailors, when confronted with a choice of two different rigs, what we'd like is a simple direct answer to the question "which is better?" Unfortunately, the answer usually is, "it depends". And not only does it depend on the geometry and construction of the sail itself but it also depends strongly on where you put it with respect to mating sails and hull(s) as well as the hydrodynamic characteristics of the hulls or hydrofoils you use it with. So a direct answer is frequently too simple.

On the other hand, only two factors are required in assessing rig performance by itself: the total aerodynamic force attainable; and the corresponding drag angle.* And so, as a problem of design optimization sailing vehicle rig selection is not all that complicated and, after a little sorting out, it's usually easy to isolate the really significant factors. The present paper represents an effort to set up a system for evaluating significant factors. In the present case, the authors have selected a particularly simple example to work with; namely, the C-class catamaran since we're familiar with the practical aspects of the problem in this context. However, the present system (or a similar one) should work effectively

---

*A remaining factor to be determined in any practical case is the point of application of the aerodynamic force with respect to the center of gravity of the vehicle into which the rig is put but we'll handle that separately.

THE EVALUATION OF SAILING VEHICLE RIG POLARS
FROM TWO-DIMENSIONAL WIND TUNNEL DATA

W. S. Bradfield
and
Lee M. Griswold

Abstract

An analysis of sail section performance differences based on wind tunnel observations and including previously unpublished section data is presented. A straightforward engineering approach to high performance sailing vehicle rig performance prediction is proposed as a design tool and examined in the context of the section data. As an application of the method, performance changes are predicted in a C-class catamaran corresponding to certain state of the art rig geometry changes. The paper is presented in two parts. Part 1 deals with sail section characteristics. Part 2 treats the evaluation of three dimensional flow effects on a rig of given section characteristics.

in almost any sailing situation.

The first requirement is a practical (preferably proven) and sufficiently sophisticated sailing yacht performance prediction method. By sufficiently sophisticated we mean that it has to be able to give us detailed reliable information about the interactions among rig, hull, and boards and rudders which really dictate the limitations on the operation of the rig. Theoretically speaking, there are a number of solidly based prediction methods available at the present time [for example, 1, 2, 3, 4]*. They're not all easy to apply. However, the advent and widespread application by sailors of the programmable pocket calculator is rapidly making these formerly rather cumbersome calculation methods readily available to practically every sailor. One of the simpler methods [2] has in fact already been programmed for the Texas Instruments SR52 pocket calculator. The more sophisticated theory of Riise [1] has been used successfully in the Univac 1110 [5] and in the IBM 370-158 in a comparison between predicted and measured performance of C-class catamarans. It's also been used successfully in many applications to handicapping in the Pacific Multihull Association [PMA]. It will be used here (in Part 2) to implement the rig selection process in the context of the performance of the sailing vehicle into which it is to fit.

The second requirement for sailing vehicle rig selection is knowledge of the significant aerodynamic parameters (previously

*Numbers in brackets designate references at end of paper.

mentioned) as a function of rig geometry. This information falls naturally into two compartments: i) differences in rig performance due to sail section shape; and ii) differences in rig performance due to planform and installation geometry. In what follows we shall deal with these in the order noted above. Specifically, we will rely on wind tunnel data from two-dimensional rigid sail models to evaluate effects of section shape. This is justified by comparison with full scale performance [2,5,24] in the case of fully battened unarigs and wing sails. Additionally, as the present example we have chosen an aerodynamically simple "high performance" sailing vehicle; i.e. one which normally sails faster than wind speed and tacks downwind. These vehicles never operate with the rig fully stalled. At the present time, this class includes ice boats, land yachts, D-class and C-class catamarans and Tornados. Monohull unarigs also fit into this general class but it becomes necessary to complicate the program by including heeled hull resistance curves as well as stalled operation of the rig downwind because they're not "high performance" vehicles. Stalled performance was worked out, by the way, in reference [2] for a slow multihull but will not be done here since C-class rigs do tack downwind.

Differences in unarig performance due to differences in planform may be evaluated using data which has accumulated in the practical aerodynamics of light airplanes (for example [17,18,21]) as the present example will show. Except for a major difference in normal operating camber range, the other design factors are about

the same, namely: planform differences; aspect ratio variations;
deck seal configurations (wing-fuselage interactions); and windage
(parasite drag) effects. Multiple element unarigs (flapped and/or
slatted) can be handled quite nicely in the same vein (see the
configuration of Figure 3, for example). On the other hand, the
performance of traditional multiple element rigs (like the sloop
rig; main plus drifter; main plus spinnaker; etc.) mounted on
monohulls is much more difficult to predict and, particularly, to
test experimentally. Although progress continues in this area [4,6,7],
full scale performance data comparable to that available for multihulls
has not yet accumulated and traditional monohulls are considered of a
difficulty beyond the scope of the present paper.

Finally, before getting started with the analysis proper,
it's necessary to define "optimum performance". We'll do so first
for the sailing vehicle and then for the rig in sailing vehicle
context. Of course, optimum performance depends on what sailing
conditions you have in mind. In what follows we assume 'round the
buoys racing conditions--a smooth sea and moderate to light winds;
specifically, winds under 25 knots and $[a/LWL] \gtrsim 0.10$.* For the
vehicle our aim will be to select the rig so that we obtain the
greatest possible value of $[V_b/V_\tau]$ at every heading τ and windspeed
V_τ; viz., maximum boat speed under all conditions. For the rig this
means attainment of maximum useable thrust compatible with the design
heeled and pitched hull characteristics. In other words, the vehicle

*See Nomenclature for definitions of symbols.

must be powered to the design limit of heeling and/or pitching at all times. If vehicle stability is not limiting, then the rig power utilized may be limited by consideration of pinching or by critical Reynolds number flows in very light air. Obviously, if you sheet the rig until the boat pinches, pitchpoles, or capsizes you've overpowered it. Practically speaking, operating within these vehicle imposed constraints simply means that we rarely use the full potential power of the rig even in light air. The optimum useful power is what we're after in rig selection or design. Clarification of this concept requires more precise definition of the forces and moments involved.

The Sailing Envelope Concept

Figure 1 is a sketch of the type of rig which we've chosen to analyze. Details of the aerodynamic force components are shown on Figure 2. It is easy to show from the geometry of Figure 2 that the thrust coefficient is

$$C_T = C_{R_a} \sin(\beta - \delta_a) \tag{1}$$

And it follows that the maximum value of thrust on any heading β to the apparent wind will be obtained by maximizing C_{R_a} (i.e., the total force developed by the sail) and minimizing δ_a (the angle at which it leans back from a perpendicular to the apparent wind direction as shown in Figure 4). The constraints on the maximization are those vehicle imposed constraints which we just mentioned above. But we don't have to worry about those until later in the anlaysis. For the present we simply look for those section characteristics which will give us maximum aerodynamic force (C_{R_a}) and minimum drag angle (δ_a) for any selected sail section shape and all possible sailing conditions.

Some sail section shapes currently in use on C-class catamarans are shown in Figure 3, (see also reference [8]). In Figure 4, recent data [10] from subsonic wind tunnel measurements of the aerodynamic force and drag angle of the circular arc shape with a cylindrical mast are shown. The 17% camber chosen is toward the high side in the range of commonly used sail cambers (.05 < h/c < .25). Corresponding values of C_{R_a} and δ_a are shown for two angles of attack:*
that which gives minimum drag angle $\delta_{a\,min}$ (dashed line), and that which produces the maximum sail force $C_{R_{a\,max}}$ (heavy line) at this camber. One observes that they are quite different angles of attack (2° vs. 15°) for this case. This is true in general for conventional sail section shapes. The reason is that the maximum sail force for conventional section shapes is frequently developed after appreciable flow separation has occurred and flow separation is the greatest contribution to increased section drag angle. Note that the correct geometrical relationship among apparent wind vector, sail section chord line, and aerodynamic resultant force vector is shown on Figure 4 for $\alpha = 15°$ including the point of application of the force to the sail. The position of the point of application of the force vector $\vec{C}_{R_a}$ is obviously the determining factor in respect to helm balance. We'll see later how important this can be to overall performance by hooking the leech of a sail and comparing its effect on the performance of a C-cat with that of an "unhooked" leech.[†] From

*Note from Figure 2 that the angle of attack $\alpha = \beta - $ [leeway + boom angle to vehicle centerline] but we don't have to worry about that explicitly as we'll see later.

[†]See Appendix 1.

equation (1) we concluded that

$$C_{T_{max}} = C_{R_{a_{max}}} \sin(\beta - \delta_{a_{min}}) \qquad (2)$$

but it's obvious from Figure 4 that $C_{R_{a_{max}}}$ does not correspond to $\delta_{a_{min}}$ in this case. We can choose either $\delta_{a_{min}}$ or $C_{R_{a_{max}}}$ but not both. A trivial calculation using equation (1) will show that from Figure 4, if $\beta \approx 45°$ (apparent close reach), $C_{T\delta_{a_{min}}} = 0.98$ while $C_{TR_{a_{max}}} = 1.11$; i.e. $C_{R_{a_{max}}}$ is the better choice. If you're close hauled ($\beta \approx 20°$) $C_{T\delta_{a_{min}}} = 0.45$ and $C_{TC_{R_{a_{max}}}} = 0.43$ and $\delta_{a_{min}}$ is the better choice. If $\beta = 23°$, $C_{T\delta_{a_{min}}} = C_{TC_{R_{a_{max}}}} = 0.52$ so it doesn't matter. It's safe to conclude from this that if you're close hauled you should shoot for $\delta_{a_{min}}$ but if you're not, it's better to let your leeside telltales fly a little and go for $C_{R_{a_{max}}}$. On the other hand, trying to conclude too much from a single camber is a temptation to be avoided. For example, who sails closehauled with 17% camber? What we can safely conclude from Figure 4 is: i) $\delta_{a_{min}}$ and $C_{R_{a_{max}}}$ usually don't correspond for a given sail section configuration; ii) which factor is more critical so far as thrust is concerned depends on which leg you're sailing; and iii) a single camber is not enough to show the whole picture even for two-dimensional wind tunnel data.

Figure 5 shows what happens as you change the camber from zero to 18% with a "clean" leading edge (no mast) and a circular arc section. These data are taken from references 10, 11, 12 and 13. Each symbol of one type on the figure represents a different angle of attack at a given camber as in Figure 4. Different symbols represent different cambers. Also, each angle of attack symbol can represent

different apparent wind angles, boom angles, and leeway angles as
shown on Figure 2. And so Figure 5 can be pretty complicated unless
we concentrate simply on achieving the maximum thrust attainable with
the circular arc section for all sailing conditions as before. Then
it becomes quite simple because what we helmsmen generally do is
trim to the maximum tolerable total sail force ($C_{R_{a_{max}}}$). The vehicle
(boat, hydrofoil, land yacht,--whatever) response imposes the sail-
force limit. Then in order to get maximum thrust out of this
vehicle limited sailforce, we choose a camber (outhaul; downhaul;
mast bend; etc.) which will give us the minimum drag angle ($\delta_{a_{min}}$).
As an example, if the boat has limited us to $C_{R_a} = 1.2$ (see, for
instance: Table 1, column (5); $\beta = 16.1$), Figure 5 shows that the
best camber is 10% ($\delta_{a_{10}} = 1.72°$)--18% camber is too much ($\delta_{a_{18}} = 5.51°$)
and 6% is too little ($\delta_{a_6} = 2.33°$) in this 10 knot breeze. From these
data, then [see equation (1)]: $C_{T_{10\%}} = 0.30$; $C_{T_{6\%}} = 0.29$; and
$C_{T_{18\%}} = 0.22$.* The same procedure works to provide maximum thrust
for all available values of C_{R_a}. The dashed line indicates the locus
of all such points for all the cambers shown on Figure 5. This is
the curve the expert helmsman will trim to by the seat of his pants.
We have called it the "sailing envelope". An important thing is that
with it we can calculate performance without explicit consideration
of individual camber curves which greatly simplifies matters.
Effectively, we let the boat choose the best camber.

---

*Note that the horizontal scale of Figure 5 is magnified to separate
 the camber curves.

Examples of sailing envelopes for different sections are shown as Figures 9 and 10 which we'll discuss in detail a little later on. These envelope polars serve as input data for the vehicle performance calculations.

Notice that maximum thrust is not the only benefit we reap by choosing sail trim as just described. Choosing $\delta_{a_{min}}$ also implies obtaining the minimum possible heeling force for a chosen thrust; i.e., along the sailing envelope, maximizing the thrust at a point automatically gives you the minimum heeling force you can get with that section shape and those sailing conditions. This is because from Figure 2

$$\frac{C_H}{C_T} = \cot(\beta - \delta_a)$$

and so for a given heading β to the apparent wind minimum drag angle δ_a gives the least heeling force for a given value of thrust. This beneficial effect of "aerodynamic cleanliness" on heeling force is equally as important as the effect on thrust so far as overall performance is concerned, qualitatively speaking, and certainly cannot be ignored quantitatively (see, for example, [2]).

Maximizing Thrust by Choice of Sail Section Geometry

Aerodynamic cleanliness for a sailing rig means minimal aerodynamic drag which implies minimum drag angle, viz.,

$$\delta_{a_{min}} = \sin^{-1}[C_{D_{a_{min}}}/C_{R_a}] \tag{3}$$

where

$$C_{D_a} = C_d + C_{D_\pi} + C_{D_i}.$$

C_{D_π}, the parasite drag, and C_{D_i}, the induced drag are not chargeable

to sail section characteristics and will be dealt with in Part 2 under rig performance considerations. C_d is the sail section drag coefficient (usually called profile drag) and includes friction drag and drag due to flow separation. Of these two, drag due to flow separation is by far the more serious consideration in sail sections. To put it another way, if the main object in shaping rig planforms is to minimize induced drag at high sail loadings (and we'll see that it is) then the main object in shaping sail sections is to minimize flow separation at high section loadings. With this end in view, this section of the paper will be devoted to the discussion of some effects of maximum camber location, camberline shape, mast shape, and use of wingsail sections on flow separation control (i.e., profile drag) of sail sections. More detailed information will be found in reference [10] (see also references [13 and 14]).

Figure 6 shows some effects of changing the location of the maximum camber position at constant camber (7½%) on sail section performance characteristics. Compared are a circular arc, the upper half of a NACA 0015 section, and the same section with the luff and leech positions reversed as shown on Figure 6 to provide a hooked leech model. These models were all fabricated from sheet metal and tested in the Merrill Wind Tunnel at Cal Tech. Details are given in reference [10]. The hooked leech configuration is obviously the worst of the three. Its drag angle δ_a is the greatest at every sail force coefficient C_{R_a}. Shown are three values, $C_{R_a} = 0.8$; 1.1; and 1.4. Corresponding values of δ_a, $\Delta C_T/C_T$, and $\Delta C_H/C_H$ are shown on Figure 6 for the extreme cases. Table 1, column (5), guided the choice of β

values for use in making these example calculations [equation (1)]. They correspond to close hauled and close reaching headings with respect to the apparent wind. For broader headings, larger sail coefficients and, therefore, higher cambers would be in order. In Figure 6, the effect of the hooked leech is to increase the drag angle at every value of sail force coefficient as the table of values shows. This results in corresponding poorer performance of the hooked leech section with respect to thrust and heel force. To look at it positively, by eliminating the hooked leech you get a thrust gain plus a decrease in heeling force at every value of sail force C_{R_a}. The center of effort of the section will also move forward as you eliminate the hook from behind the midchord point to between the 25% and 40% chord point for the [0015/2] shape [10]. So far as the data of Figure 6 are concerned there is little difference between the circular arc and the [0015/2]. The center of effort of the [0015/2] will be a little farther forward and the section will stall a little sooner. In summary, as you move your maximum camber aft at constant camber you add drag, the center of effort moves aft, and the sail stalls sooner if you have a hooked leach. The center of effort movement will probably affect helm balance adversely and thereby increase the vehicle drag (see Part 2).

From Figure 6 we can at least conclude that the maximum camber position should be somewhere between the 20% chord point and the midchord point. The next question is "what is the best sail section shape?" Figure 7 compares data from three typical shapes

with the maximum camber forward. One of these is the [0015/2] also
plotted on Figure 6. A difference is that to each of the shapes shown
on Figure 7 a mast has been added (for details, see Figure 3). The
effect on the [0015/2] model of adding the mast was to slightly
increase the drag angle (decrease the thrust) at each value of sail
force coefficient. In fact, we'll see that this is generally the case
for all sail sections (Figure 8). The position of maximum camber for
all three shapes on Figure 7 is very close to 30% chord. A comparison
similar to that which we made for Figure 6 will show the [0015/2] to
be the worst shape for $C_{R_a} < 1.10$. The Eipper hang glider wing section
shape with its reflexed run is as good as the parabolic for $C_{R_a} < 1.0$
but flow separation on the leeside [10] rapidly develops for $C_{R_a} > 1.0$.
The "parabolic" shape, essentially a parabolic section forward with a
flat run aft, provides the highest value of thrust (lowest δ_a) with
the least heeling force for values of $C_{R_a} \gtrless 1.35$. Before reaching
the stall at $C_{R_a} = 1.35$ one would trim for a lower drag angle at a
higher camber as we did in the example of Figure 5 and so that part
of the Figure can be ignored. Summarizing Figure 7, it would appear
that the best of the three section shapes for minimizing separation
(hence, δ_a) is the parabolic entry and the flat run. The best sailing
envelope will come from the section that consistently gives $\delta_{a_{min}}$ at
the highest C_{R_a} for every camber that we can trim to. Looking at just
one camber as we have on Figure 7 doesn't necessarily give us the
total answer as to section shape. However, it gives a good indication.

The circular cylinder mast section when applied to the
[0015/2] was shown to decrease its performance. One might expect the

mast installations on the other two shapes to be equally harmful. The data of reference [10] shows that this is indeed the case. Figure 8 is a comparison of a number of different mast configurations on a circular arc sail section shape at two different cambers. Considerable previous work has been published bearing on this mast question (see, for example, references [13 - 19]) which should be summarized at the outset. On the negative side, the aggregate data show that cylindrical masts are always harmful in their effects on sail section performance and that the tangent-mast configuration of Figure 4 is the least harmful of circular cylinder sections. The data also show that if you insist on separating the flow at the leading edge of your sail by installing a non-rotating cylindrical mast you can minimize the separation by moving your maximum camber aft as you sail free (and probably unbalance your helm). So here is one case where moving maximum camber aft is quasi-helpful. But it's better for sail section performance to eliminate the leading edge separation by streamlining the mast and rotating it and to keep the maximum camber forward as in Figure 6. The data from reference [15] on 31 different combinations of mast shape, sail camber and mast rotation clearly show the possibilities of sail leading edge control by shaping and rotation of standard (and some not so standard) mast extrusions.

The present investigation [10] extended previous observations by making comparisons between clean leading edges (Figure 5), tangent mast installations, and wing masts for different section shapes. Some of the data are shown as Figure 8. The intent of Figure 8 is

to compare the effects on sail section performance of adding a nicely faired and rotatable wing mast to a sail section leading edge which originally had no leading edge fairing at all. Sketches of the compared configurations are shown on the figure. The sail section shape chosen is a circular arc and two different cambers are used to give an idea of the sailing envelope characteristics. The dashed line is the sailing envelope as defined on Figure 5; i.e., the locus of sail trim points which will give minimum drag angle (maximum thrust) at every value of sail force coefficient attainable with cambers between 9% and 15%. You will notice that the envelope includes several different leading edge configurations. If $C_{R_a} = 0.65$ it indicates that the small wingmast and low camber will be about as good as no mast at all. The big wing mast at low camber will have more drag than the little wing mast--but not much. If $C_{R_a} = 1.1$ the unfaired leading edge has a clear advantage. If $C_{R_a} = 1.5$ the big wing mast at 15% camber is the best choice. If $C_{R_a} = 1.8$, either no fairing at all or the 40% chord wingmast fairing will serve equally well. Reference to Table 1 will give a good idea of what apparent headings (β) call for these magnitudes of sail coefficients for a C-class catamaran in a 10 knot breeze. Obviously, conditions will be different for different boats.

What's the point of Figure 8? The main point is that leading edge separation is a serious problem so far as sail section performance is concerned. Calculation of a table like that shown in Figure 6 will quickly show how serious it is. A second point is that practically

any mast you use to hold the sail up with is going to be harmful to performance even if it's rotatable. And, thirdly, the data of Figure 8 indicate that the biggest wingmast tried is the best aerodynamic compromise over the entire range of sail force for the circular arc sail section configuration. This naturally leads us to the consideration of full chord wing masts, i.e. wingsails.

Figure 9 is a comparison of some familiar wing sail section shapes. In order to achieve the equivalent of high soft sail camber it is necessary to use flaps on a wing, as every sailor knows. With this in mind, we have included the sailing envelope of the 40% wing mast sail section of Figure 8. We simply regard it as a wing with a 60% chord dacron flap. The data are taken from reference [10]. Compared with it are data from a NACA 23012 section with 25% chord plain flaps [23] and the circular arc section data from Figure 5.

On Figure 9 the data are divided into regimes by magnitudes of sail force coefficient C_{R_a}. Sailforce coefficient values below about 0.50 are rarely used but the data indicate that when they are, the flapped wing will have the advantage due to weatherside separation of the other shapes. For true wind values between 12 knots and 22 knots and with C-cats, values of C_{R_a} between 0.50 and 1.00 will frequently be called for beating and close reaching. Figure 9 shows that the flapped wing still holds a clear superiority (and for the same reason) in this regime so far as drag angle is concerned. Hence, the flapped wing is again the logical aerodynamic best section among the three sections presented. In the intermediate range of sail coefficients $(1.0 < C_{R_a} < 1.5)$ there really isn't much choice. The

flapped wing holds a very slight advantage but, percentagewise, it will be essentially negligible.after the induced drag and the parasite drag of the rig are added later on. However, for ($1.5 < C_{R_a} < 2.0$) the situation changes as the leeside surface stall sets in and the leeside telltales begin to fly free. Notice that the 15% camber wing mast has an apparent advantage in this regime but that it stalls "hard" when leeside separation does occur. The flapped wing in order to reach these sail coefficients requires 10° to 30° flap angle with the attendant leeside trailing surface separation and that penalizes its performance. The circular arc with no mast has a "soft" stall (the C_{R_a} keeps rising as α is increased) but the drag angle increases very rapidly to high values. In summary, Figure 9 shows that it's easy to make a reasonably shaped sail section work well in the midrange of sailforce coefficients ($0.9 < C_{R_a} < 1.8$) if you don't insist on using a fixed circular mast or standard mast extrusion at the leading edge. For values of $C_{R_a} > 1.8$ and $C_{R_a} < 0.9$ either leeside or weatherside (for non-wings) separation will set in and increase the drag angle thereby decreasing the thrust available and increasing the heeling force at a given sail force.

In winding up this section, it is of interest to take a brief look at what is being done at present to improve the situation shown on Figure 9. The aerodynamics technical literature is full of information on wing section performance characteristics. Most of these sections, however, were developed for best performance at low cambers. References [17,18 and 21] are probably familiar to most technically oriented sailors. Less familiar are comparatively

recent reviews of developments in the area of high lift, high lift/drag ratio flying machine aerodynamics [20,22] which bear directly on high performance sailing rig development because "high lift, high lift/drag" means large sail force and small drag angle simultaneously which is what we seek. In the interest of pointing out the present state of the art with respect to sail section development, Figure 10 compares three good wing sections (two of which are currently in use on C-class catamarans) with the circular arc section sailing envelope of Figure 5. A fourth equally important example is the three element wing section of Patient Lady's III and IV (reference [8]) shown on Figure 3. However, there is no section data on this configuration at this time. We will in Part 2 compare some of the data of Figures 9 and 10 corrected to aspect ratio 4 with the aspect ratio 4 data of reference [8].

Figure 10 summarizes the spread in section performance of currently in use and/or available sails. Note that the profile drag scale (C_d) has been expanded to emphasize the differences in drag angle (δ_a). A table comparing thrust coefficients and heeling force coefficients for selected values of β is shown on the figure. Sketches of five sections are shown. Data from only four of them appear as mentioned above. Patient Lady's section is included only in the interest of completing the spectrum of configurations available.

Also shown for the first time (in this paper) is section data

from a high C_{R_a} low δ_a shape due to Liebeck (reference [9]) as an example of how far we have to go in developing non-separating sail shapes. Notice that this single element fixed camber section equals or exceeds the performance of all the sail sections currently in use over the entire practical present day working range of sail force.* Flow separation control for these shapes (see also references [10,20,22]) is by surface curvature control. And in putting them to practical use as sails a determining factor will be how simply yet precisely we can control the section shape as we run through a range of cambers. If we can control them we can expect improvements over the best circular arc section of as much as those shown in the table of Figure 10.

Summary and Conclusions

A system for sailing rig selection or design must start with a consideration of sail section performance characteristics. What we've tried to do in Part 1 is to pull together and summarize available wind tunnel and water tunnel data bearing specifically on sail section performance as contrasted to the performance of airfoils or hydrofoils which usually are designed to operate most efficiently at low values of lift coefficient. We have pointed out that the challenge in sail section performance improvement is essentially in preventing flow

---

*The authors have taken the liberty of indicating on the sketch how this might be converted to a wing-mast-with-dacron-flap configuration.

separation at large values of sail force and at small values as well. The intermediate range is apparently not a serious problem. We have isolated what we believe to be the most significant geometric variables and have shown some data (Figures 4 through 9) to quantify the relative importance of each. On Figure 10 we've tried to summarize the available spectrum of section shapes in a way that shows the comparative improvement in performance as successively larger areas of flow are prevented from separating at the high and low ends of the sail force range. Finally, the question as to whether all this available sail section refinement is going to be worth the trouble and expense for a given application cannot be answered until three dimensional flow effects are accounted for, attendant weight penalties of a chosen section are evaluated, and so on. These aspects of the problem are tackled in Part 2 of the paper.

Part 2

Rig Planform and Installation Effects

The end product of the first step in rig design evaluation was a section sailing envelope covering all anticipated unstalled sailing conditions for a selected section geometry (Figure 10). The second step consists of adding the aerodynamic effects of making a working rig installation out of the selected sail section. Everything we do from now on will detract from the performance indicated on Figure 10; i.e., for a given sail section, the performance shown on Figure 10 is as good as it's going to get. To put it still another way, every step that we take in converting a sail section to a rig results in adding aerodynamic drag. Added drag at constant C_{R_a} means a larger drag angle which means diminished thrust and increased heeling force as we demonstrated in Part 1. In sail section configuration design or selection the factors of major importance were presented in Part 1 as maximum camber location; sail section shape; mast configuration; and thickness distribution (for wing configurations). We argued that flow separation control is the name of the game-- especially at the highest values and the lowest values of sail force coefficient (C_{R_a}).

In real rig installations additional flow separation results directly from air flow about the hull(s); standing and running rigging; deck fittings; crew; etc. These effects we lump under "windage" or "parasite drag". Also, "induced drag" results from flow around the head and foot of the sail due to the pressure drop from weather to

lee side. Both theoretical and empirical evaluations of induced drag are thoroughly discussed in the sailing technology literature. For example, see references [8,14,16,17,18,21,25,26,27,28,29,30] some of which include large amounts of parasite drag data. And it's not our intention to try to add anything to that information--except the small amount of new information on "end plate" effects shown on Figure 14. The end plate effect at the foot of the sail comes from the proximity of the rig to the sea surface and tends to decrease the induced drag to the degree that the configuration inhibits flow around the foot (see Figure 1, for example). We will also get a little information about masthead endplates from Figure 14.

Summarizing, our aim in Part 2 is to show what the added aerodynamic drag due to the real rig effects described above does to sail section performance (compare Figures 10 and 17) and, consequently, to sailing vehicle performance. In doing that, we'll restrict ourselves mainly to data from generally available references like [17,18,21] and standard practical aerodynamics "handbooks" like [25]. In other words, our intent is to make the conversion from section polar to rig polar as simply as possible consistent with obtaining engineering accuracy from our sailing vehicle performance predictions. By "engineering accuracy" we mean accuracy consistent with the experimental uncertainty of full scale performance measurements to date. Finally, we'll compare our results with available C-class measured performance and suggest some improvements in the prediction method.

The Aerodynamic Model

Before we get into the details of section data conversion,
we have to decide what to do about the natural wind velocity profile.
Every sailor knows that the wind speed increases from the sea surface
to the masthead [37]. But most of us don't know what to do about it.
To quote meteorologist-sailor Alan Watts [31]: "It is a platitude
that the wind increases from the surface upwards. What is not so
certain is how it increases." It has been established in the last
fifty years that how it increases depends mainly on the sea (or land)
surface roughness and the degree of atmospheric instability. However,
details of the dependence are very much a subject of current meteoro-
logical investigation (for example, [32,33,34,37]). It follows that
general statements about the detailed shape of the profile are con-
jectural in view of the present state of the art; therefore, to assume
much detail in a wind profile model proposed for general application
is to assume more than we know at present. Nevertheless, the wind
profile exists and attempts to evaluate its effects on rig aerodynamics
have been made since at least the time of Manfred Curry [36]. Examples
of different models used comparatively recently are given in
references [18,14,35].

Our view of the simplest profile tolerable for the present purpose
coincides with the approximation of Riise [1]; namely, i) zero relative
wind velocity at the sea surface; ii) a linear increase to "true wind
velocity" at deck level, iii) constant velocity from deck level to

masthead; and iv) "true wind velocity" defined as the velocity

measured at 40% of the mast height (approximate sail center of

effort). This straight line profile model is shown on Figure 11

compared with a recently measured Long Island Sea Breeze profile [34].

The equation which is currently used to describe the sea breeze family

of profiles is shown on the plot. Empirically determined quantities in

the equation are: u_* ∿ the "friction velocity", which varies with

atmospheric stability; z_0 ∿ the "surface roughness length", which

depends on the sea state; and κ ∿ "von Korman's constant", determined

from turbulent boundary layer velocity profile measurements. If you

know values of u_* for stable, unstable, and neutrally stable atmos-

pheric conditions and values of z_0 for sea states you're likely to

encounter then you can predict the velocity variation from sea surface

to masthead. However, sensitivity of the wind profile to these factors

is not small (for example, reference [31], pp. 125,126) and, in view of

the general uncertainty with respect to which model to choose for a

given calculation, Riise's model appears to us a reasonable across the

board approximation.

With the straight line model, obviously we're simply ignoring the

wind velocity gradient from the deck level up. This simplifies the

calculations but it ignores the effect of the wind gradient on aero-

dynamic twist $\beta(z)$ and load distribution $[\Delta R_a/R_a{}^*]$ from foot to head

of the sail. Typical magnitudes of these effects are shown on Table 3

for close hauled and downwind courses for the boat of Table 2 in

10 knot and 15 knot breezes. The wind profile equation used is the

sea breeze profile equation of Figure 11. For comparison, the straight

line profile values are found at z = 15 ft in Table 3. It is clear from these data that both twist and vertical aerodynamic loading variation are appreciable. For a soft sail we can assume that sail twist can be controlled to compensate for the aerodynamic twist by letting the leech fall off. In the case of a wing sail, flap deflection will be varied from foot to head to compensate. Hence, aerodynamic twist due to the natural wind can probably be safely ignored as a first approximation.

On the other hand, the vertical load distribution $[\Delta R_a(z)/R_a{}^*]$ varies quite a bit with heading to the wind and with the mean wind speed as well. In general, the result of the straight line assumption will be an overestimation of the total sail force generated and an under-estimation of the induced drag. As the net effect, an overprediction of the available thrust should be expected. There will also be a tendency to underpredict the height of the sail center of effort slightly. In view of aeronautical engineering experience, it would seem reasonable to counter these effects by an empirically determined aspect ratio correction. However, the authors at present know of little data bearing on this question and so a quantitative evaluation will not be attempted. This is a matter which requires further investigation.

Parasite Drag Prediction

Having selected the true wind velocity profile model, the second step is to define the rig in terms of the geometry of the boat. For this example we use the sketch of Figures 1 and 12 as the model. We

define the "rig" as including everything above the sailing waterline; i.e., everything that can possibly add aerodynamic drag is charged to the rig. Working from the waterline up to deck level, we'll consider the parasite drag first.

The prediction of parasite drag is based on the concept of "equivalent flat plate area" of the dragging surface--a sort of "will this surface as seen by the apparent wind have as much drag as a signboard of equivalent area?" concept (for example, [14], p. 103). The numbers are determined from either full scale or model experiments [17,18,25]. We will adopt the concept as formulated by Riise [1] for the present calculations.

Looking down from the masthead of the boat of Figure 12 we have

Case 1 (light air)

Case 2 (flying hull)

Plan View   Side View
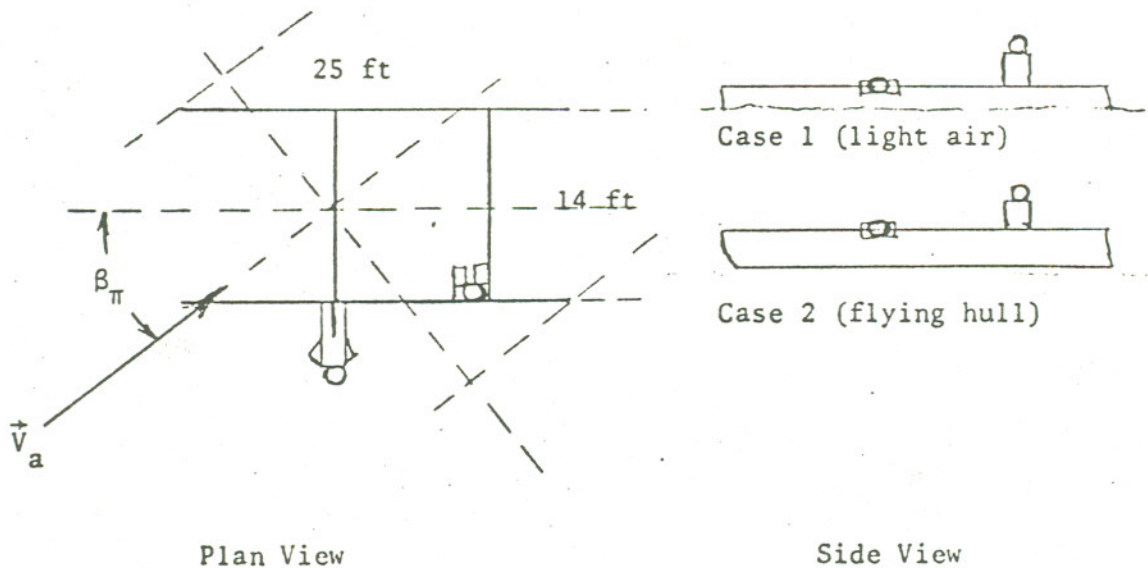
the view shown above. The major "signboard" areas are:

Hull(s) (topsides) = A_{TS}; sideview projection

Crossmember projected area = A_{XM}; forward projection

Crew projected area = A_{PC}; forward projection.

Standing and running rigging parasite drag is neglected.

It follows that

$$D_\pi = [A_{TS} \sin \beta_\pi C_{D_{\pi TS}} + A_{XM} \cos \beta_\pi C_{D_{\pi XM}} + 2A_{PC} \cos \beta_\pi C_{D_{\pi PC}}]$$
$$\times [\tfrac{1}{2}\rho_{air} V_{a\pi}^2] \tag{4}$$

where $V_{a\pi}$ is the mean apparent wind speed between sea surface and deck (Figure 12); and

β_π is the corresponding angle for $V_{a\pi}$ to the boat heading. Values for $C_{D_{\pi TS}}$, $C_{D_{\pi XM}}$ and $C_{D_{\pi PC}}$ are found in reference [18] (Chaps. 3, 4 and 13). An overall parasite drag coefficient may be defined by

$$C_{D_\pi} = \frac{D_\pi}{\tfrac{1}{2}\rho_a V_a^2 A_s} \tag{5}$$

where D_π is obtained from equation (4). Due to the variation of projected areas with heading to the apparent wind, C_{D_π} varies with heading. Typical variation is shown on Figure 13. These calculations are for the boat of Table 1 of configuration Figure 1. For this case the range is from $C_{D_\pi} = 0.055$ closehauled to $C_{D_\pi} = 0.125$ tacking downwind. The ratio of sail section drag to parasite drag coefficient is also shown both for the boat of Table 1 and for that configuration with a sail of Liebeck section (Figure 10). For the circular arc section, parasite drag and section (profile) drag are of the same order for most of the headings. For the Liebeck section, the profile drag averages only about 15% to 25% of the vehicle parasite drag. Jumping ahead a bit, the ratio of induced drag to parasite drag for the rig of Table 1, Figure 1 is also shown on Figure 13. For this general configuration (boat of Figure 1 and rigs of Figure 16), the induced drag and parasite drag are roughly equal except when broad reaching. We conclude that the profile (sail section) drag, the parasite drag, and the induced drag are of equal practical importance

so far their effects on the vehicle rig polar are concerned.

Induced Drag Prediction

As we pointed out earlier, the induced drag results from the tendency of the air to flow around the head and foot in response to the pressure drop from weather to leeside. The series of sketches on Figure 14 is intended to illustrate the gross features of what happens when you convert from a sail section configuration (Figures 3 and 14a) to a cantilevered 3-dimensional sail model (Figures 3 and 14b). If you subsequently add an end plate at the "head" of the model sail, you have the situation shown as Figure 14c. The corresponding measured effects [10] on the sail section polar are shown as Figure 15. Comparing configurations 14a and 14b shows a decrease in $C_{R_{a \, max}}$ of about 6% and an increase in drag angle at $C_{R_{a \, max}}$ of $\Delta\delta_a = 5.9°$. The comparative effect on thrust available is shown on Figure 15. As the data shows, the section considered has a very low drag angle at $C_{R_{a \, max}}$ which tends to magnify the relative importance of the drag angle increase due to the induced flow (compare sections of Figure 10). The increase is significant for all sections, however, and it can be predicted which means we can account for it in our rig designs. Before we leave Figure 14 to discuss details, we'd like to point out that Figure 15 shows that putting a one chord length diameter end plate on the head of the sail model (Figure 14c) helped quite a bit despite the added profile and junction drag [18].

We mentioned that the induced drag can be predicted and we should have added--with the help of empirical corrections [18,25]. We have that for a rig

$$C_{D_a} = C_d + C_{D_\pi} + C_{D_i} \tag{6}$$

where section drag C_d and parasite aerodynamic drag C_{D_π} have already been discussed. The induced drag depends strongly on the aerodynamic load distribution ($\Delta R_a/R_a{}^*$, Table 3) up the mast. If the load distribution is elliptical we have from Prandtl and Munk [38] that

$$C_{D_i} = \frac{C_C{}^2}{\pi \, AR} \tag{7}$$

and this implies an elliptical planform (Figures 1 and 16). For non-elliptic planforms, a theoretical correction factor was devised early on by Glauert [39]; specifically, for rectangular and tapered planforms.

Through the years this has been modified by comparison with experiments in NASA and other experimental facilities. A compilation of such results is to be found in reference [25], Chapter 9 and in reference [18], Chapter 7. A typical useful corrected form of equation (7) is

$$C_{D_i} = \frac{C_C{}^2}{e_s \, \pi \, AR} \tag{8}$$

where $C_C = C_{R_a} \cos \delta_a$; (Figure 2)

e_s = "sail efficiency factor";

$(e_s \, AR)$ = "effective aspect ratio".

In specific cases, e_s is obtained by comparing measured values of induced drag like those to be found on Figure 15 with values predicted from equation (7) using the geometric aspect ratio of the model. In Figure 15, it turns out that $e_s = 0.73$ gives a good fit of equation (7) to the data.

The final three dimensional flow effect to be considered is the "end plate" effect illustrated in Figures 14 and 15. This effect is

also discussed thoroughly from a practical viewpoint in references [18]
and [25] for many different configurations. As an illustration, the
rectangular model of Figures 14 and 15 is useful. We note in Figure 14b
that the induced flow at the foot is completely blocked by the tunnel
wall. This effectively doubles the aspect ratio from 3.5 measured to
7.0. Since e_s = 0.73 from the data, $\mathcal{R}_{eff}$ = 0.73 x 7 = 5.1. Adding the
end plate decreases the drag angle and slightly increases $C_{R_{a\,max}}$. In
this case, it restores the effective $\mathcal{R}$ to that of the elliptic load
distribution; namely, $\mathcal{R}_{eff}$ = 7 as you can quickly check using equations
(7) and (8) and the data of Figure 15. So the end plate does help in
steady state conditions if it's big enough, and the question is whether
it helps enough to justify the complication and weight aloft in the
normally unsteady conditions we encounter. In any event, there's plenty
of data available in the literature cited to permit the designer-sailor
to make his own evaluation.

Comparative Rig Evaluation

Now we have pulled enough information together to permit us to make
a comparative evaluation of the rigs of Figure 16 on C-class catamaran
hulls. We will also add data on the rig of Patient Lady II (reference [8])
corrected to an appropriate effective aspect ratio (see Figures 3 and 10).

We begin with the sail section sailing envelope data from Figure 9.
This gives us the profile drag C_d over the range of C_{R_a}'s available for
both the soft sail and the flapped wing.

The second step is the evaluation of the aerodynamic induced drag
term in equation (6). We selected planform geometry and end plate effects

as the significant factors. For the soft sail, Figures 1 and 16 provide
a practical summary of the pertinent geometric features. The planform
is nearly elliptical but it has a cutout at the foot. A deck seal is
provided and so end plating results to an extent limited by trampoline
construction and hull flying. Also, experience shows that soft sail
deck seals frequently don't work as well as they're supposed to. This
means that some judgment based on experience has to be brought into play
at this point not only as to what the effective "gap" at the sail foot
may be but also with respect to which handbook geometry [17,18,25] most
closely represents the rig being evaluated. Your judgment is probably
better than ours for the cases that you're evaluating and ours is
probably better than yours for the present cases. In any case, detailed
instructions for and examples of the evaluation of C_{D_i} (i.e. $\mathcal{R}_{eff}$) are
found in the handbooks [17,18,25] along with the necessary data and those
are the procedures we used for the soft sail and the flapped wing of
Figures 3 and 16 starting from the section data of Figure 9. The final
values of the effective aspect ratio ($\mathcal{R}_{eff}$) which we arrived at are
shown on Figure 16 for these two cases.

Figure 16 also shows the planform geometry of the multiple element
section shown on Figure 3 (Hubbard wing). The multiple element model was
tested at a finite aspect ratio [8] and, therefore, the profile drag
cannot be separated out of the experimental results. However, since it's
assumed that profile drag is unaffected by aspect ratio changes (in the
range of our interest) the data taken at the model $\mathcal{R} = 2.5$ can be corrected
to an aspect ratio more compatible with the geometry of Figure 16 by

standard methods ([40], Chapter 6C). Specifically,

$$C_{D_{i2}} = C_{D_{i1}} + \frac{C_C^2}{\pi}\left(\frac{1}{\mathcal{R}_2} - \frac{1}{\mathcal{R}_1}\right) \tag{9}$$

where, for this case, $\mathcal{R}_1 = 2.5$ and $\mathcal{R}_2 = \mathcal{R}_{eff} = 6$. The uncertainty in the correction for Patient Lady's geometry was sufficient to allow us to place it squarely in the middle of the $\mathcal{R}_{eff}$ spread between the Aquarius V and Miss Nylex values--an example of the practical judgment mentioned earlier.

That takes care of the first and the last terms of equation (6). The remaining term is the parasite drag coefficient C_{D_π} which we've already discussed and evaluated (Figure 13). Since we have deliberately ignored the contributions of standing and running rigging for the present cases, the form of the parasite drag expression [equation (4)] is the same for all three rigs.* We have, so to speak, simply selected a pair of hulls and fitted the three different rigs in succession to that one hull(s) configuration for performance evaluation. It's clear from equation (6), Tables 2 and 3, and Figures 12 and 13 that the parasite drag depends very much on the specific performance of the vehicle and must, therefore, be evaluated in the context of vehicle performance predictions. We have selected a mean value from Figure 13; namely, $C_{D_\pi} = 0.1$ for inclusion on Figure 17 which shows the rig polars for the geometries of Figure 16.

Figures 17 and 18 together represent the final result of our rig

---

*The inclusion of a rigging drag term in equation (6) although simple to do would have complicated matters in the present example and, in any event, the added drag was considered negligible.

polar evaluation. Figure 17 is the 3-dimensional rig polar, as we just said, and Figure 18 is the comparative performance evaluation of the three rigs over the design spectrum of operating conditions. Neither figure gives complete information by itself and, furthermore, trouble shooting on details requires "subsystem" information like that printed out on Tables 1 and 2. However, much of the performance information is summarized on the figures.

For example, the results plotted on Figure 18 indicate a clear aerodynamic advantage for Patient Lady's wing over the other two configurations; especially, at high sail force coefficients. For values of $C_{R_a} > 1.3$, Figure 17, the advantage begins to appear. The induced drag and the parasite drag of the three rigs are equal, practically speaking, over the entire sail force operating range. The difference is in the profile drag due to flow separation--especially at high values of the sail force coefficient. What the figure tells us is just what we should have suspected: the multiple element wing is more successful in avoiding leeside-trailing-surface separation than is the wing with plain trailing edge flaps and therefore it's a better thruster at high sail force coefficients.

The next practical question is: how often is the vehicle operation going to call for such high sail force coefficients? We discussed this matter in Part 1 of the present paper and also in reference [5]. The quickest way to get an answer is by examining Figure 18 where the comparative performance of the three rigs is plotted over the design spectrum of operating conditions. It's appropriate here to point out that in computing

the performance, we've kept the hull weights and crew weights the same but we've added realistic (according to our present information) sail structural weight increments for the two wing sails (see Figure 16 for numbers).

The plots on Figure 18 clearly show the situation with respect to sail force operating range. In light air (5 knots) where heeling stability permits all the boats to call for the highest values of sail force coefficient the Patient Lady rig's combination of high sail force and low drag angle permits maximum utilization of her inherent aerodynamic advantage and she is far and away the best performer. Hull flying begins to limit $C_{R_{a\,max}}$ in $V_\tau = 10$ knots wind and the advantage decreases. Note that as a result of Nylex's weight penalty she and the soft sailed boat are neck-and-neck in this wind range. As the wind goes up to 15 knots and 20 knots, the heavier boats have a double advantage: i) they're "stiffer" due to their weight increment (some detail is given on this point in reference [5]); and ii) they're also "cleaner" aerodynamically speaking. And so the rigs have sorted themselves out very logically in the light of the aerodynamic information on Figure 17 and what we know about the effects of all up weight changes on the performance of these particular hulls [1,5].

Summary and Conclusions

In Part 1, we isolated and gave some data to evaluate what we believe to be the most significant geometric variables affecting sail section performance. We also summarized the available spectrum of sail section shapes in a way that shows the comparative improvement in performance

that results by eliminating flow separation at the high and low ends of the section performance polar (Figure 10). We promised that in Part 2 we would evaluate three dimensional effects, attendant weight penalties of a chosen section, and "so on". By "so on" it turns out that we meant wind strength and headings (Figure 18). We have concluded that sail section profile drag, parasite drag (or windage), and rig induced drag are all equally important to rig performance evaluation. None should be neglected without careful consideration. The section profile drag can be evaluated from available wind (and water) tunnel data for many sail sections now in use. Ample parasite drag data is available in the aerodynamics handbooks but parasite drag effects on the rig must be evaluated in the context of vehicle performance calculations. Plenty of induced drag data is also available in the literature but some caution should be reserved (by aerodynamicists, at least) in applying aspect ratio corrections to the highly cambered and zero thickness shapes which we use for sails because of the assumption generally used that profile drag is independent of aspect ratio. We've thrown caution to the winds in this instance. Finally, we've proved once more (at least to our satisfaction) that the cleanest rig is the best rig all other things being equal and that sometimes it pays to add weight to get aerodynamic cleanliness if all out speed is what you want.

Acknowledgments

References

1. Riise, H. N., "Optimized Hull Length for a D-Class Catamaran", Proceedings, First AIAA Symposium on Hydronautics of Sailing, pp. 171-194, Los Angeles, California, 1969.

2. Bradfield, W. S., "Predicted and Measured Performance of a Daysailing Catamaran", Marine Technology, Vol. 7, No. 1, January 1970.

3. Myers, H. A., "Theory of Sailing Applied to Ocean Racing Yachts", Marine Technology, Vol. 12, No. 3, July 1975.

4. Letcher, J. S., Jr., "Optimum Windward Performance of Sailing Craft", J. Hydronautics, Vol. 10, No. 4, October 1976.

5. Bradfield, W. S. and Madhavan, S., "The Predicted and Measured Performance of Two C-Class Catamaran Rigs", State University of New York at Stony Brook, CEAS Report #279, June 1976.

6. Kirkman, K. L. and Pedrick, D. R., "Scale Effects in Sailing Yacht Hydrodynamic Testing", Transactions of SNAME, Vol. 82, 1974.

7. Clauser, M. U., "The Tow Testing of Full Scale Yachts", Sixth AIAA Symposium on the Aero/Hydronautics of Sailing, Vol. 15, January 1975.

8. Scherrer, J. O., "Aerodynamics of High Performance Wing Sails", Marine Technology, Vol. 11, #3, July 1974.

9. Liebeck, R. H., "A Class of Airfoils Designed for High Lift in Incompressible Flow", J. Aircraft, October 1973.

10. Bradfield, W. S., Griswold, L. M. and Clauser, F. H., "Wind Tunnel Section Data for Highly Cambered Rigid Sail Models through the Critical Reynolds Number Range", State University of New York at Stony Brook, CEAS Report #284, May 1977.

11. Milgram, J. H., "Section Data for Thin, Highly Cambered Airfoils in Incompressible Flow", NASA CR-1767, July 1971.

12. Wallis, R. A., "Axial Flow Fans", Academic Press, New York, 1961.

13. Chapleo, A. W., "A Review of Two-Dimensional Sails", S.U.Y.A. Report No. 23, University of Southampton, April 1968.

14. Marchaj, C. A., "Sailing Theory and Practice", Dodd, Mead and Company, New York, 1964.

15. Bethwaite, F. P., Mansfield, C. D., Smith, E. J., Thorne, C. P., "Wind Tunnel Tests on Over-rotating Spars of Different Types", Department of Aeronautical Engineering, University of Sydney, Australia, 1969.

16. Kay, H. F., "The Science of Yachts Wind and Water", John deGraff, New York, 1971.

17. Hoerner, S. F., Borst, H. V., "Fluid-Dynamic Lift", Hoerner Fluid Dynamics, New Jersey, 1975.

18. Hoerner, S. F., "Fluid-Dynamic Drag", Hoerner Fluid Dynamics, New Jersey, 1965.

19. Parham, H. J., Farrar, A., Macalpine-Downie, J. R., "Class-C Racing Catamarans", Transactions RINA, 1968.

20. Liebeck, R. H., "On the Design of Subsonic Airfoils for High Lift", Douglas Aircraft Co., Paper No. 6463, 1976.

21. Abbott, I. H., von Doenhoff, A. E., "Theory of Wing Sections", Dover Publications, New York, 1949.

22. Smith, A. M. O., "High Lift Aerodynamics", AIAA Paper No. 74-939 (Wright Brothers Lecture), 1974.

23. Ames, M. B. J., "Wind Tunnel Investigation of Two Airfoils with 25% Chord and Plain Flaps", NACA TN763, May 1949.

24. Bradfield, W. S., "Comparative Performance of the Flying Fish Hydrofoil and the Tornado Catamaran", Proceedings Third AIAA Symposium on Aero/Hydronautics of Sailing, Vol. 10, 1971.

25. Wood, K. D., "Technical Aerodynamics", University of Colorado, Boulder, 1965.

26. Prandtl, L., Tietjens, O. G., "Applied Hydro- and Aeromechanics", Dover Edition, 1970.

27. Milgram, J. H., "Sail Force Coefficients for Systematic Rig Variations", SNAME, Technical and Research Report R-10, September 1971.

28. Myall, J. O., Berger, S. A., "Recent Progress in the Analytical Study of Sails", AIAA Second Symposium on the Hydronautics of Sailing, Proceedings, Vol. 9, 1970.

29. Sparenberg, J. A., Wiersma, A. K., "On the Maximum Thrust of Sails by Sailing Close to Wind", Journal of Ship Research,

Vol. 20, No. 2, June 1976.

30. Letcher, J. S., Jr., "Optimum Windward Performance of Sailing Yacht Craft", Jour. of Hydronautics, Vol. 10, No. 4, October 1976.

31. Watts, Alan, "Wind and Sailing Boats", Quadrangle Books (One Design and Offshore Yachtsman), 1967.

32. Bradley, E. F., "A Micrometeorological Study of Velocity Profiles", Quart. J. R. Met. Soc., Vol. 94, pp. 361-379, 1968.

33. Taylor, P. A., "Wind Profile Development Above a Locally Adjusted Sea Surface", Boundary Layer Met., Vol. 2, pp. 381-389, 1972.

34. Stern, Mark, "The Non-Dimensional Wind Shear and Lapse Rate over Water in the Sea Breeze", Ph.D. dissertation, State Univ. of New York at Stony Brook, 1977.

35. Milgram, J. H., "The Analytical Design of Yacht Sails", Transactions SNAME, 1968.

36. Curry, Manfred, "Yacht Racing", Charles Scribner's Sons, New York, 1936.

37. Hirsch, R. F., "Is There a Velocity Gradient?", Sail Magazine, January 1974.

38. Karman, T., "Aerodynamics", Cornell University Press, 1954.

39. Glauert, H., "Aerofoil and Airscrew Theory", Cambridge University Press, 1937.

40. Prandtl, L. and Tietjens, O. G., "Applied Hydro- and Aeromechanics", Dover, New York, 1971.

AQUARIUS V

TRUE WIND VEL = VT = 10.00 KTS
SAIL AREA =, 300.00 SQ FT
AVE CREW WT = 315.00 LBS
OVER-ALL LENGTH= 25.00 FT
DISPLACEMENT = 750.00 LBS
BOARD-RUDDER CHORD= 1.00 FT
RUDDER LENGTH = 1.70 FT
SF TO LIFT HULL= 510.85LBS
RUDDER FORCE/SF = .00
NUMBER IN CREW = 1.
HYDROFOIL AREA = .00 FT
MIKING DISTANCE = 3.00 FT SQ FT

1. BOARD-RUDDER,FOIL-ARE NACA-0012 AIRFOIL SECTIONS
2. BOARD-RUDDER SECTION DRAG-NACA TN 1945 P53,FIG11
3. SAIL DRIVE POLAR OF AQUARIUS V
4. CATAMARAN HAS ZERO LEEWAY ANGLE
5. RUDDER AND DAGGERBOARD ON WEATHER HULL ARE RETRACTED
6. HYDROFOIL IS PLACED AT BOTTOM OF LEEWARD DAGGERBOARD
7. DGRBD OPERATES AT MAX L/D IF LENGTH IS LESS THAN 5 FT
8. WINDAGE AREA-SQFT-CREW = 3.CROSSBARS= 7.HULLS = 20.
9. VA FOR WINDAGE CALCULATION=VECTOR SUM VT*VTC+VB,   VTC = .5
10. CENTRE OF EFFORT ABOVE WATER =16.99
11. HYDROFOIL ASPECT RATIO =   .0
12. PROJECTED CABIN AREA = 0.

(1) τ	(2) β	(3) V_h	(4) V_a	(5) C_{R_a} SAIL COEF	(6) Q AIR	(7) Sail Force LBS	(8) Wind -age LBS	(9) Heel Force LBS	(10) Q WATR	(11) (Daggerboard) COEF	(12) Lnght FT	(13) Drag LBS	(14) (Stbd Hull) Disp LBS	(15) Drag LBS	(16) (Port Hull) Disp LBS	(17) Drag LBS	(18) Drag Rud LBS	(19) Hydro -foil Lift LBS	(20) Thrust LBS	(21) Upwd Dnwd Comp KT	(22) V_b/V_τ	(23) τ DEG
DEG	DEG	KT	KT																			
30	15.1	9.8	19.3	1.36	1.251	510	16	502	277	.455	4.00	26	790	42	0	0	2	0	58	8.530	.98	30
35	16.1	11.6	20.6	1.22	1.447	529	20	519	386	.319	4.00	24	790	54	0	0	3	0	103	9.519	1.16	35
40	17.4	12.9	21.5	1.12	1.569	527	24	514	470	.275	4.00	23	790	64	0	0	4	0	116	9.628	1.29	40
45	18.8	13.9	22.1	1.06	1.665	529	27	513	551	.235	4.00	23	790	72	0	0	5	0	128	9.622	1.39	45
55	21.0	15.6	22.9	1.00	1.762	524	32	512	699	.186	4.00	24	790	88	0	0	7	0	152	8.971	1.56	55
65	23.0	17.1	23.0	1.00	1.822	546	36	516	833	.175	3.54	26	790	101	0	0	8	0	174	7.214	1.71	65
75	24.5	18.2	23.0	1.03	1.792	553	38	518	950	.171	3.25	27	790	117	0	0	9	0	193	4.718	1.82	75
85	26.6	19.0	22.2	1.08	1.679	544	39	504	1031	.160	3.10	27	790	126	0	0	10	0	204	1.655	1.90	85
95	27.7	19.8	21.4	1.19	1.556	555	39	511	1110	.150	3.10	28	790	137	0	0	11	0	216	1.726	1.98	95
105	28.6	20.3	20.2	1.35	1.387	501	37	515	1150	.143	3.10	29	790	144	0	0	11	0	223	5.259	2.03	105
115	29.7	20.1	18.3	1.63	1.175	554	33	511	1152	.145	3.10	29	790	141	0	0	11	0	215	5.486	2.01	115
120	31.4	19.2	16.6	1.97	.933	554	29	518	1050	.161	3.10	28	790	129	0	0	10	0	197	5.585	1.92	120
125	36.6	16.6	13.6	2.03	.641	391	22	353	804	.144	3.10	20	598	79	191	35	8	0	168	5.619	1.66	125
130	41.0	15.2	11.7	2.12	.463	294	17	257	682	.138	3.10	15	482	60	307	42	6	0	142	9.783	1.52	130
135	45.1	14.1	10.0	2.12	.339	214	14	180	569	.142	2.30	11	395	43	395	43	5	0	117	9.977	1.41	135
140	53.3	12.4	8.0	2.15	.218	140	10	106	442	.113	2.10	7	395	34	395	34	4	0	92	9.530	1.24	140
145	65.5	10.8	6.7	2.16	.135	87	6	53	333	.115	1.45	4	395	27	395	27	3	0	69	8.847	1.08	145
145	65.7	10.8	6.3	2.17	.134	86	6	52	331	.115	1.44	4	395	27	395	27	3	0	69	8.835	1.08	145

Table 1. Aquarius V Performance at V_τ = 10 knots
(reference [5]).

AQUARIUS V PERFORMANCE   HULL DRAG 10/20*CHORD

TRUE WIND VEL = VT = 10.00 KTS
SAIL AREA =, 300.00 SQ FT
AVE CREW WT = 315.00 LBS
OVER-ALL LENGTH= 25.00 FT
DISPLACEMENT = 790.00 LBS
BOARD-RUDDER CHORD= 1.00 FT
RUDDER LENGTH = 1.70 FT
CE TO LIFT HULL= 510.99LBS
RUDDER FORCE/SF = .00
NUMBER IN CREW = 1.
HYDROFOIL AREA = .00
HIKING DISTANCE = 3.00 FT

1. BOARD-RUDDER,FOIL-ARE NACA-0012 AIRFOIL SECTIONS
2. BOARD-RUDDER SECTION DRAG-NACA TN 1945 P53,FIG11
3. SAIL DRIVE POLAR OF AQUARIUS V
4. CATAMARAN HAS ZERO LEEWAY ANGLE
5. RUDDER AND DAGGERBOARD ON WEATHER HULL ARE RETRACTED
6. HYDROFOIL IS PLACED AT BOTTOM OF LEEWARD DAGGERBOARD
7. DGRBD OPERATES AT MAX L/D IF LENGTH IS LESS THAN 5 FT
8. WINDAGE AREA-SQFT-CREW = 3.CROSSBARS= 7.HULLS = 80.
9. VA FOR WINDAGE CALCULATION=VECTOR SUM VT*VTC+VB,   VTC = .5
10. CENTRE OF EFFORT ABOVE WATER =16.99
11. HYDROFOIL ASPECT RATIO = .0
12. PROJECTED CABIN AREA = 0.

(1) τ	(2) β	(3) V_b	(4) V_a	(5) C_{R_2} SAIL	(6) Q	(7) Sail Force	(8) Wind-age	(9) Heel Force	(10) Q	(11) (Daggerboard) COEF	(12) Lnght	(13) Drag	(14) (Stbd Hull) Disp	(15) Drag	(16) (Port Hull) Disp	(17) Drag	(18) Drag Rud	(19) Hydro-foil Lift	(20) Thrust	(21) Upwd Dnwd Comp	(22) V_b/V_τ	(23) τ
DEG	DEG	KT	KT	COEF	AIR	LBS	LBS	LBS	WATR	COEF	FT	LBS	LBS	LBS	LBS	LBS	LBS	LBS	LBS	KT		DEG
40	25.1	9.9	19.7	1.49	1.493	929	18	513	292	.459	4.00	49	790	42	0	0	20	0	130	7.607	.99	40
45	21.2	11.2	19.6	1.36	1.302	531	21	510	355	.361	4.00	48	790	51	0	0	25	0	146	7.099	1.12	45
50	22.0	12.1	20.0	1.33	1.276	544	23	519	417	.315	4.00	51	790	58	0	0	29	0	163	7.265	1.21	50
55	23.9	12.8	20.3	1.30	1.293	543	25	514	467	.279	1.00	53	790	62	0	0	32	0	176	7.350	1.28	55
65	26.3	14.1	20.5	1.51	1.322	558	27	520	568	.232	4.00	60	790	74	0	0	39	0	205	5.959	1.41	65
75	29.3	15.1	20.2	1.35	1.389	542	30	515	653	.200	4.00	64	790	83	0	0	45	0	223	3.921	1.51	75
85	39.7	15.9	19.5	1.47	1.223	570	31	516	722	.182	4.00	68	790	90	0	0	49	0	210	1.395	1.59	85
95	33.0	16.3	18.3	1.68	1.137	573	29	517	750	.175	4.00	70	790	94	0	0	51	0	246	1.412	1.62	95
105	36.0	16.9	16.4	2.03	.918	559	26	507	721	.179	4.00	68	790	90	0	0	49	0	235	4.110	1.59	105
115	42.3	14.0	13.3	2.11	.405	382	19	327	560	.150	4.00	52	567	55	222	30	39	0	193	5.917	1.40	115
125	51.0	12.4	10.5	2.14	.372	241	13	158	437	.143	3.10	37	390	34	390	34	30	0	151	7.089	1.23	125
130	57.0	11.4	9.1	2.17	.293	184	10	132	371	.117	3.10	31	395	30	395	30	26	0	128	7.321	1.14	130
135	65.1	10.3	7.9	2.17	.207	134	8	82	306	.128	2.20	24	395	25	395	25	21	0	106	7.319	1.03	135
140	74.9	9.4	6.7	2.28	.151	103	6	53	251	.107	2.10	19	395	21	395	21	18	0	88	7.324	.94	140
145	85.3	8.6	5.8	2.42	.113	81	4	35	214	.094	2.10	16	395	19	395	19	15	0	74	7.096	.85	145
150	97.6	8.0	5.0	2.43	.086	63	2	14	182	.082	1.10	12	395	16	395	16	13	0	61	6.911	.80	150
155	111.5	7.4	4.5	2.44	.070	51	1	0	156	.037	.20	10	395	13	395	13	11	0	51	6.698	.74	155
155	111.7	7.1	4.5	2.43	.070	51	1	0	155	.024	.20	10	395	13	395	13	11	0	51	6.691	.74	155
205	199.2	7.5	4.7	2.43	.071	53	2	2	161	.024	1.10	11	395	14	395	14	11	0	54	6.723	.75	205

Table 2.   Aquarius V Performance at V_τ = 10 knots with Hull Profile Drag Added to Match Observed Apparent Wind Angles.

$V_\tau = 10$ kts, $\tau = 45°$, $V_b = 11.2$ kts, $V_a* = 19.5$ kts, $\beta* = 21.0°$

(1) z (ft)	(2) $V_\tau(z)$ kts	(3) $V_a(z)$ kts	(4) $\beta(z)$ deg	(5)[†] $\dfrac{\Delta R_a}{R_a*}$ coef.
3.0	7.5	17.4	17.9	-0.20
3.5	7.8	17.6	18.2	-0.19
4.0	7.9	17.7	18.5	-0.18
4.5	8.1	17.9	18.7	-0.16
5.0	8.3	18.0	18.9	-0.15
7.0	8.8	18.5	19.6	-0.10
10.0	9.3	18.9	20.3	-0.06
15.0	9.9	19.5	21.0	0.00
20.0	10.3	19.9	21.5	0.04
25.0	10.6	20.2	21.9	0.07
30.0	10.9	20.4	22.2	0.09
35.0	11.1	20.6	22.4	0.12
40.0	11.3	20.8	22.6	0.14

$V_\tau = 10$ kts, $\tau = 140°$, $V_b = 8.2$ kts, $V_a* = 6.4$ kts, $\beta* = 84.3°$

(1) z (ft)	(2) $V_\tau(z)$ kts	(3) $V_a(z)$ kts	(4) $\beta(z)$ deg	(5)[†] $\dfrac{\Delta R_a}{R_a*}$ coef.
3.0	7.5	5.4	63.4	-0.29
3.5	7.8	5.5	65.7	-0.26
4.0	7.9	5.6	67.6	-0.26
4.5	8.1	5.6	69.3	-0.23
5.0	8.3	5.6	70.7	-0.23
7.0	8.8	5.8	75.2	-0.18
10.0	9.3	6.1	79.2	-0.09
15.0	9.9	6.4	84.3	0.00
20.0	10.3	6.6	87.2	0.06
25.0	10.6	6.8	89.4	0.13
30.0	10.9	7.0	88.9	0.20
35.0	11.1	7.1	87.6	0.23
40.0	11.3	7.3	86.5	0.30

$V_\tau = 15$ kts, $\tau = 45°$, $V_b = 12.8$ kts, $V_a* = 25.5$ kts, $\beta* = 24.2$

(1) z (ft)	(2) $V_\tau(z)$ kts	(3) $V_a(z)$ kts	(4) $\beta(z)$ deg	(5)[†] $\dfrac{\Delta R_a}{R_a*}$ coef.
3.0	11.3	22.3	21.0	-0.24
3.5	11.6	22.6	21.4	-0.21
4.0	11.9	22.9	21.6	-0.19
4.5	12.2	23.1	21.9	-0.18
5.0	12.4	23.3	22.1	-0.17
7.0	13.2	24.0	22.8	-0.11
10.0	13.9	24.7	23.5	-0.06
15.0	14.8	25.5	24.2	0.00
20.0	15.4	26.1	24.7	0.05
25.0	15.9	26.6	25.1	0.09
30.0	16.3	26.9	25.4	0.11
35.0	16.7	27.3	25.6	0.15
40.0	16.9	27.5	25.8	0.16

$V_\tau = 15$ kts, $\tau = 140°$, $V_b = 12.7$ kts, $V_a* = 9.6$ kts, $\beta* = 81.9°$

(1) z (ft)	(2) $V_\tau(z)$ kts	(3) $V_a(z)$ kts	(4) $\beta(z)$ deg	(5)[†] $\dfrac{\Delta R_a}{R_a*}$ coef.
3.0	11.3	8.3	60.9	-0.25
3.5	11.6	8.4	63.2	-0.23
4.0	11.9	8.5	65.1	-0.22
4.5	12.2	8.5	66.8	-0.22
5.0	12.4	8.6	68.2	-0.20
7.0	13.2	8.9	72.7	-0.14
10.0	13.9	9.2	77.2	-0.08
15.0	14.8	9.6	81.9	0.00
20.0	15.4	9.9	84.9	0.06
25.0	15.9	10.2	87.2	0.13
30.0	16.3	10.5	88.9	0.20
35.0	16.7	10.7	89.7	0.24
40.0	16.9	10.9	88.6	0.29

[†]Two-dimensional flow assumed, i.e. $\Delta R_a/R_a* = V_a^2/V_a*^2 - 1$

*Asterisked values are those obtained from the "straight line" velocity profile

Table 3. Effects of the Natural Wind Profile on Aerodynamic Twist and Load Distribution Up the Mast.

Figure Captions

Figure 1.   Definition of Aerodynamic and Hydrodynamic Resultant Force Vectors.

Figure 2.   Definition of Aerodynamic Force Components.

Figure 3.   Typical Sail Section Shapes.

Figure 4.   Aerodynamic Polar for a Tangent-Mast Section of 17% Camber.

Figure 5.   The Effect of Changing the Camber on the Performance of a Circular Arc Sail Section (the "Sailing Envelope").

Figure 6.   Effects of Changing the Maximum Camber Position at Constant Camber.

Figure 7.   Sail Section Shape Change Effects on the Aerodynamic Polar.

Figure 8.   Some Leading Edge Fairing (Mast) Effects on Sail Section Performance.

Figure 9.   Comparison of Sailing Envelope Characteristics of Wing Sections and Sail Sections

Figure 10.   A Sail Section Performance Spectrum from Data on Currently Available Geometries.

Figure 11.   A Typical Measured Long Island Sea Breeze Profile Compared with the Straight Line Model of Riise [1].

Figure 12.   Effects of the Natural Wind Profile on the Vehicle Apparent Wind Profile Tacking Downwind.

Figure 13.   Variation of the Parasite Drag Coefficient with Heading to the True Wind (boat of Table 1).

Figure 14.   A Qualitative Comparison of Two and Three-Dimensional Flow About Sail Models.

Figure 15.   A Quantitative Comparison of the Three-Dimensional Flow Effects (configurations) of Figure 14.

Figure 16.   Comparative Rig Planform Geometry of Three Currently Competing C-class Rigs.

Figure 17.   Rig Polar Sailing Envelopes for the Geometries of
             Figure 16.

Figure 18.   Comparative Predicted Performance of the Rigs of Figure
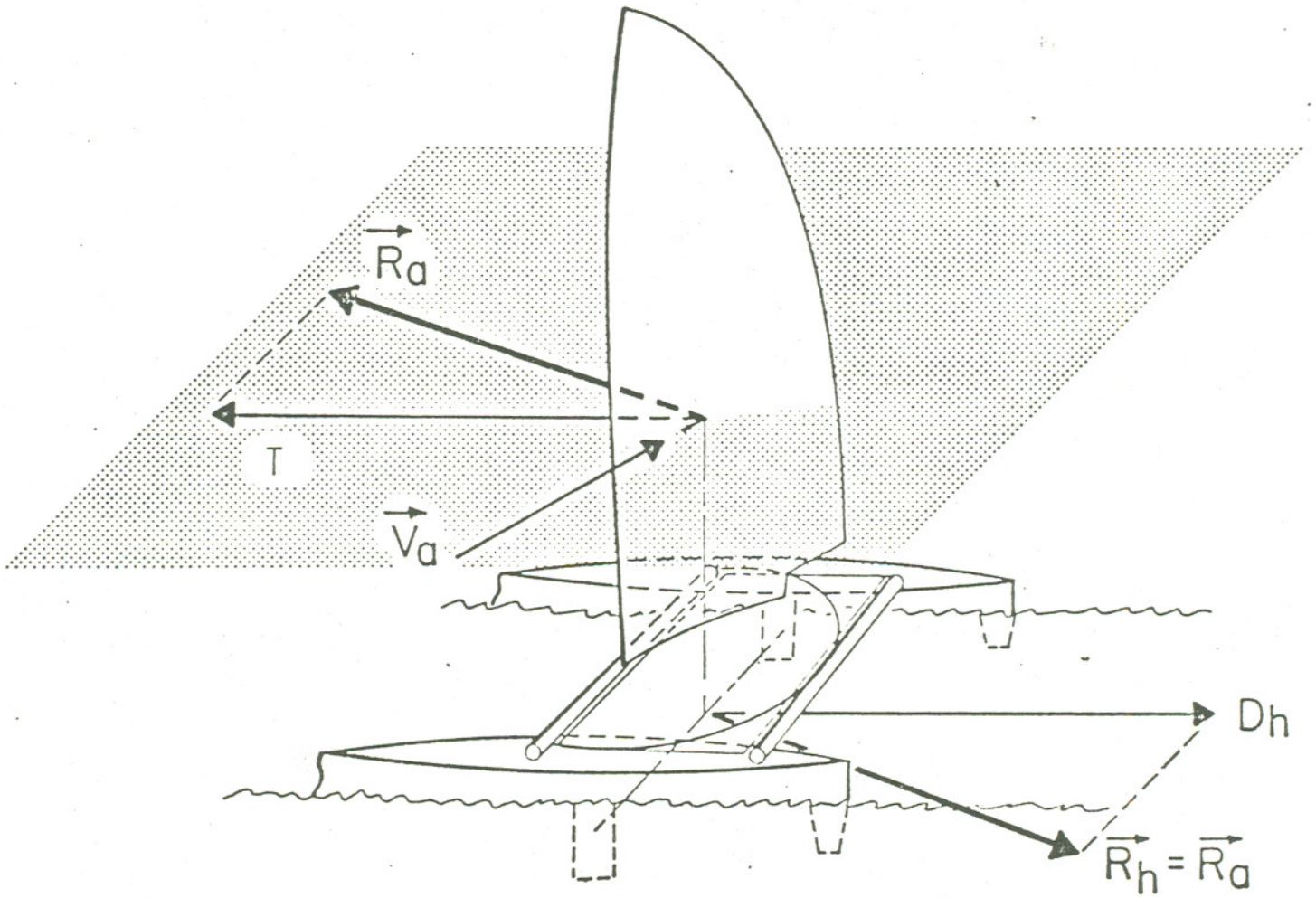   16.

Figure 1. Definition of Aerodynamic and Hydrodynamic Resultant
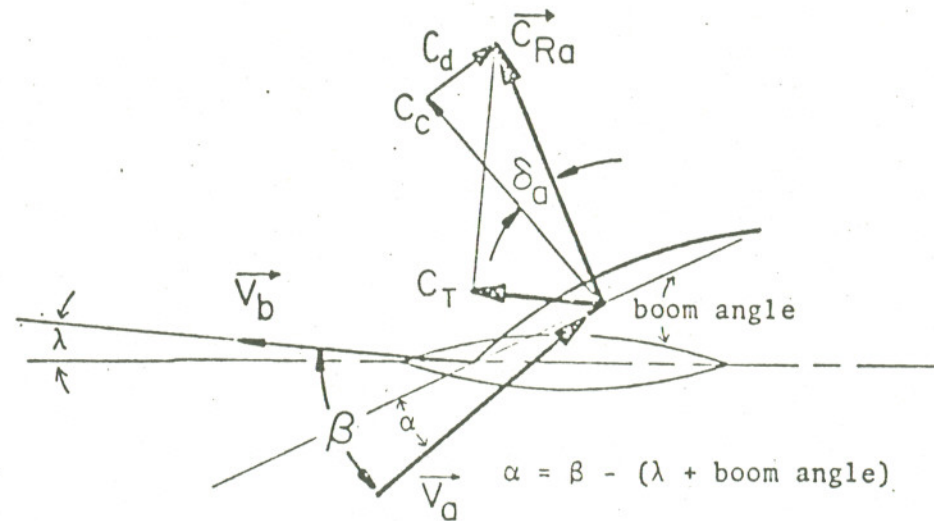Force Vectors.
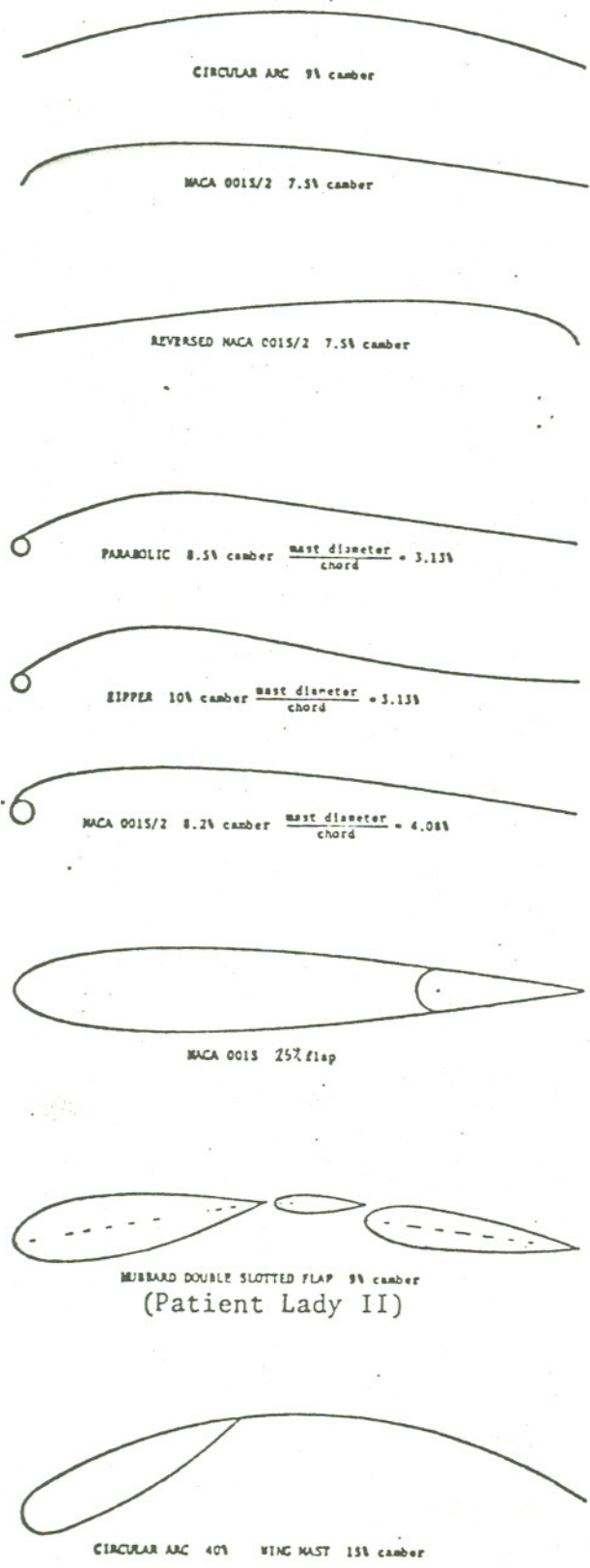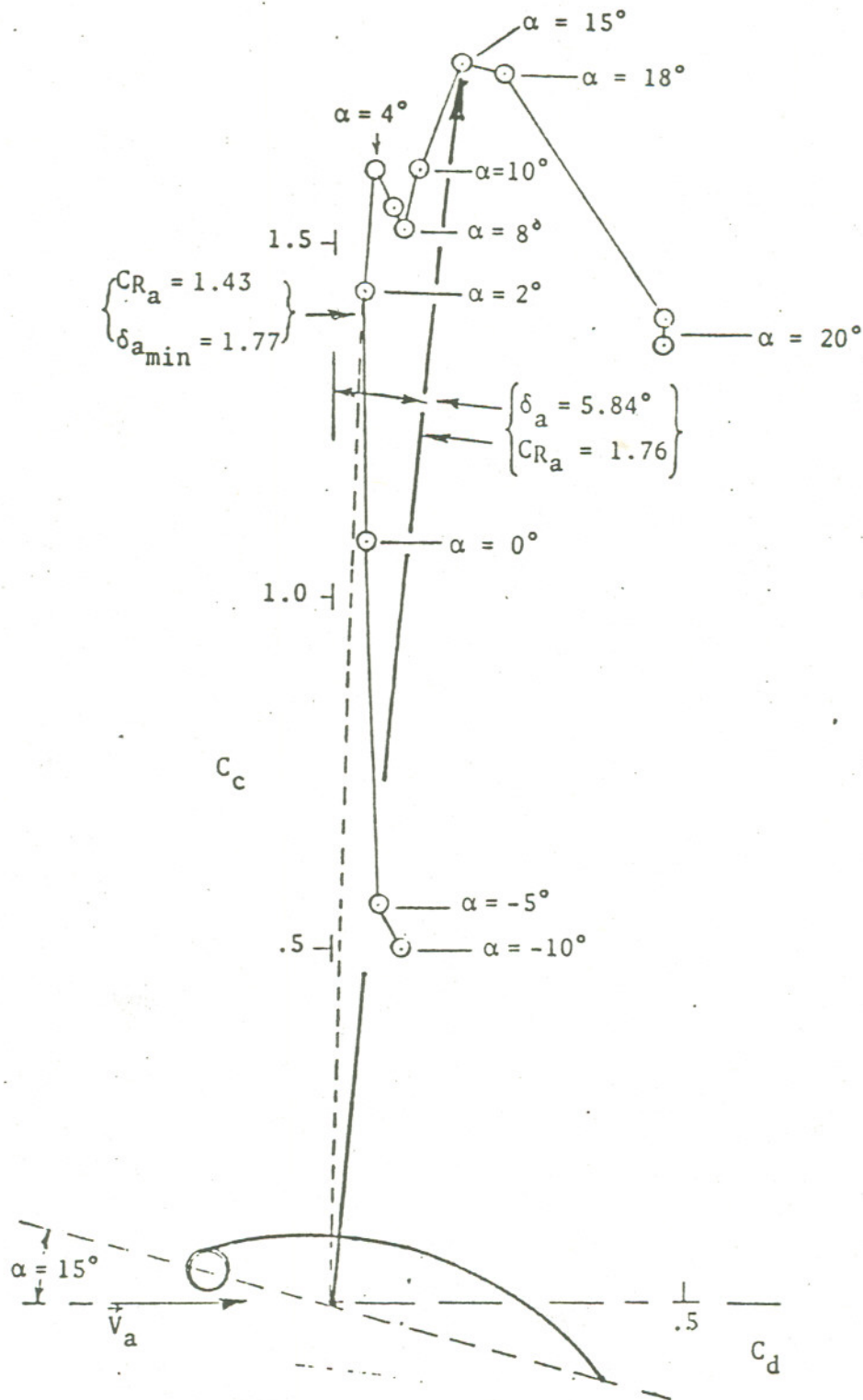
Figure 2. Definition of Aerodynamic Force Components.

CIRCULAR ARC 9% camber

NACA 0015/2 7.5% camber

REVERSED NACA 0015/2 7.5% camber

PARABOLIC 8.5% camber $\frac{\text{mast diameter}}{\text{chord}} = 3.13\%$

ZIPPER 10% camber $\frac{\text{mast diameter}}{\text{chord}} = 3.13\%$

NACA 0015/2 8.2% camber $\frac{\text{mast diameter}}{\text{chord}} = 4.08\%$

NACA 0015 25% flap

HUBBARD DOUBLE SLOTTED FLAP 9% camber
(Patient Lady II)

CIRCULAR ARC 40% WING MAST 15% camber

Fig. 3. Typical Sail Section Shapes
(Drawn to ½ scale)

Fig. 4. Aerodynamic Polar for a Tangent-Mast Section of 17% Camber
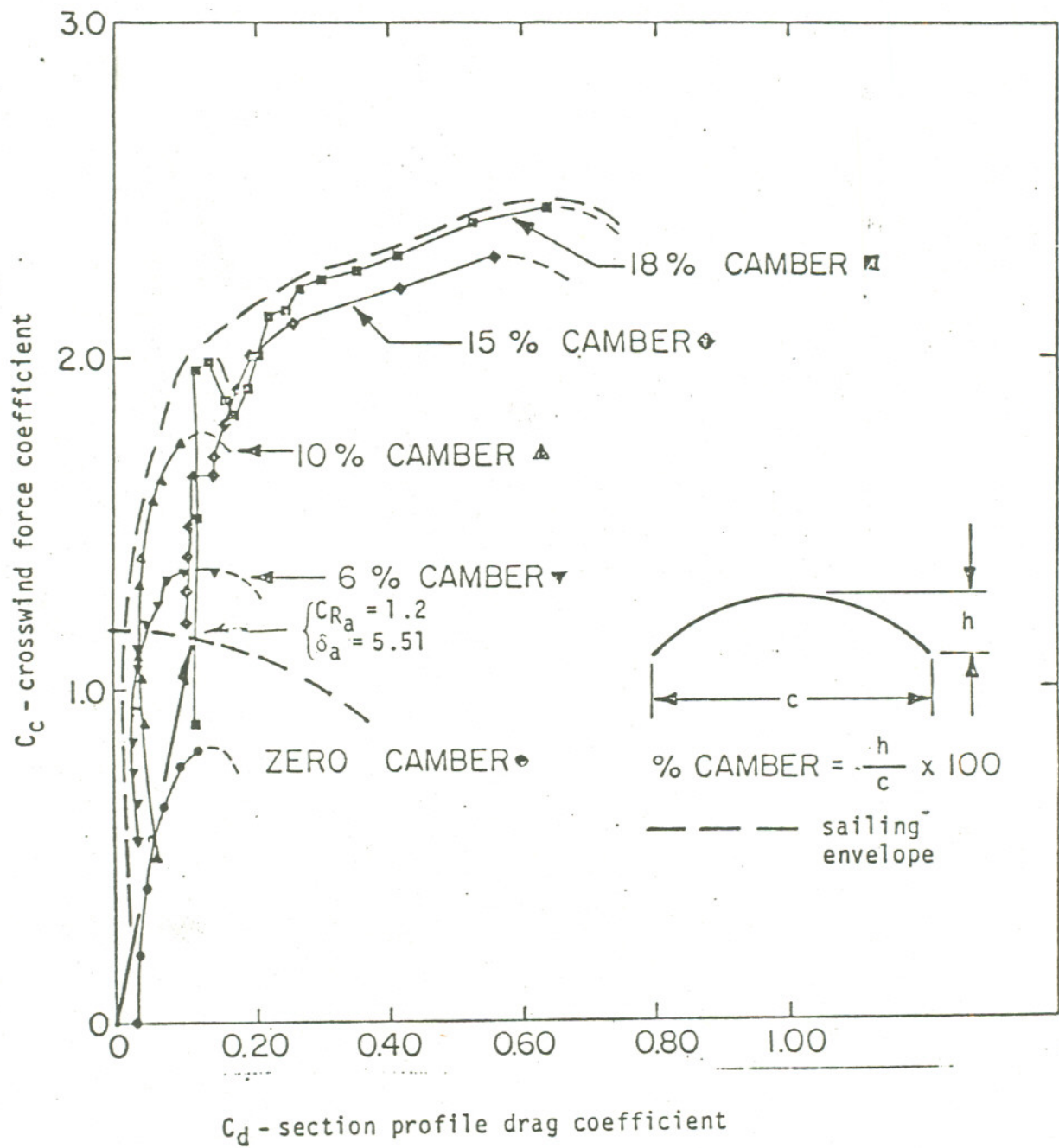
Fig. 5. The Effect of Changing the Camber on the Performance of a Circular Arc Sail Section (the "Sailing Envelope").

C_{R_a} = 1.4

C_{R_a} = 1.1

1.5

1.0

C_c

.5

circ arc

0015/2

0015/2

C_{R_a} = .8
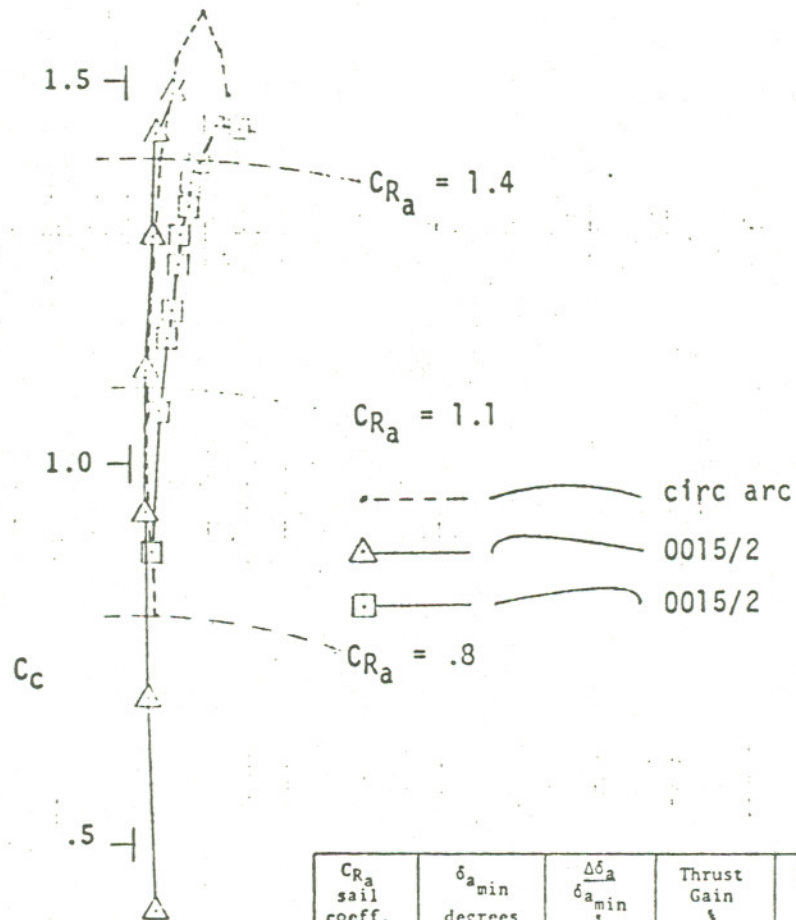
C_{R_a} sail coeff.	$\delta_{a_{min}}$ degrees	$\frac{\Delta\delta_a}{\delta_{a_{min}}}$ %	Thrust Gain %	Heel Force Decrease %	Typical ß Degrees
0.8	1.50	42.8	3.47	0.37	20
1.1	1.46	56.9	3.45	0.617	25
1.4	1.64	136.7	7.89	1.99	30

0   .2   .4   .6   .8

C_d

Fig. 6. Effects of Changing the Maximum Camber Position at Constant Camber.

Fig. 7. Sail Section Shape Change Effects on the Aerodynamic Polar

Legend:
- parabolic; straight run
- Eipper; reflexed run
- [0015/2]; curved run

NOTE: The C_d scale is doubled to separate the curves.

C_c axis values: 1.5, 1.0, .5, 0

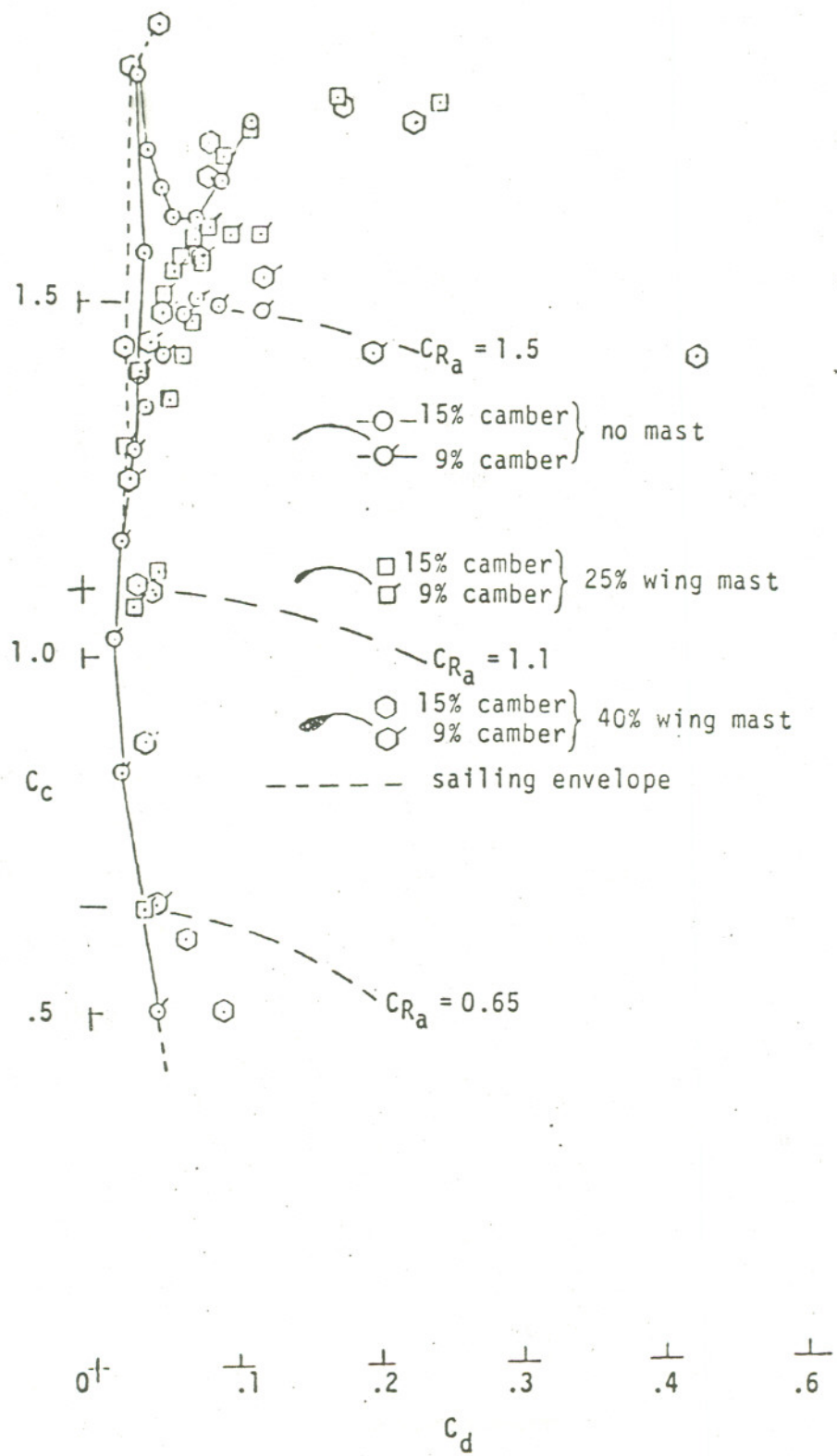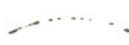C_d axis values: 0, .10, .20, .30, .40

Fig. 8. Some Leading Edge Fairing (Mast) Effects on Sail
         Section Performance.

Fig. 9. Comparison of Sailing Envelope Characteristics of Wing
Sections and Sail Sections.
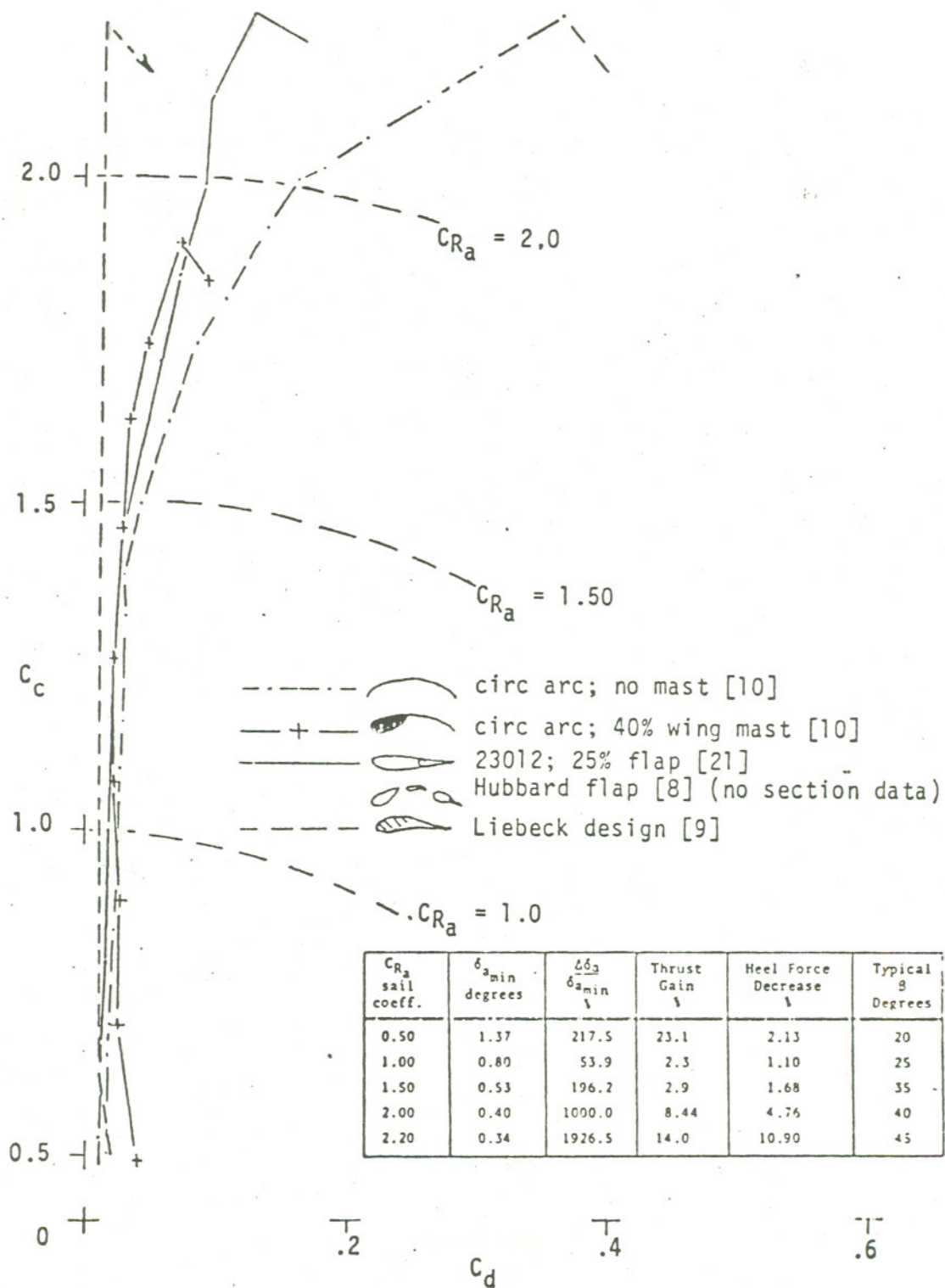
2.0 $C_{R_a} = 2.0$

1.5 $C_{R_a} = 1.50$

C_c

circ arc; no mast [10]
circ arc; 40% wing mast [10]
23012; 25% flap [21]
Hubbard flap [8] (no section data)
Liebeck design [9]

1.0 $C_{R_a} = 1.0$

C_{R_a} sail coeff.	$\delta_{a_{min}}$ degrees	$\frac{\angle\delta_3}{\delta_{a_{min}}}$ %	Thrust Gain %	Heel Force Decrease %	Typical β Degrees
0.50	1.37	217.5	23.1	2.13	20
1.00	0.80	53.9	2.3	1.10	25
1.50	0.53	196.2	2.9	1.68	35
2.00	0.40	1000.0	8.44	4.76	40
2.20	0.34	1926.5	14.0	10.90	45

0.5

0   .2   .4   .6

C_d

Fig. 10. A Sail Section Performance Spectrum from Data on Currently Available Geometries.

masthead →

$$\frac{u}{u^*} = \frac{1}{k} \ln \frac{z - z_0}{z_0}$$

$u^* = 30$ cm/sec $(\triangleq \sqrt{\overline{u'w'}})$

$z_0 = 1$cm; $k = 0.35$

—— straight line approximation

← masthead

approximate sail center of effort

40

30

20

10

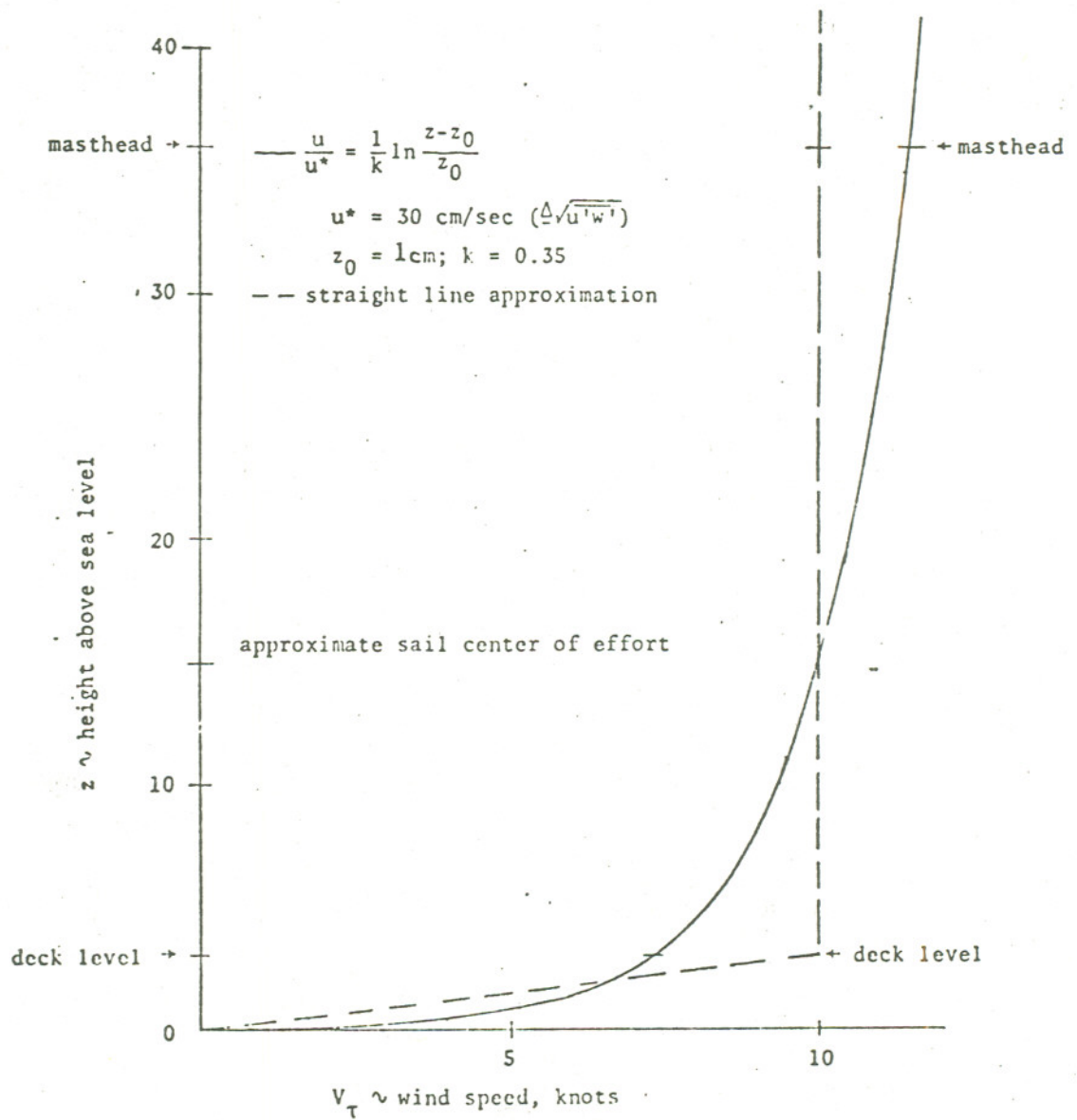z ∿ height above sea level

deck level →

← deck level

0

5

10

V_τ ∿ wind speed, knots

Figure 11. A Typical Measured Long Island Sea Breeze Profile
Compared with the Straight Line Model of Riise [1].

$V_\tau = 10$ kts; $\tau = 140°$; $V_b = 8.2$ kts; (boat of Table 2)

——— natural wind profile $V_\tau(z)$; (Table 3)

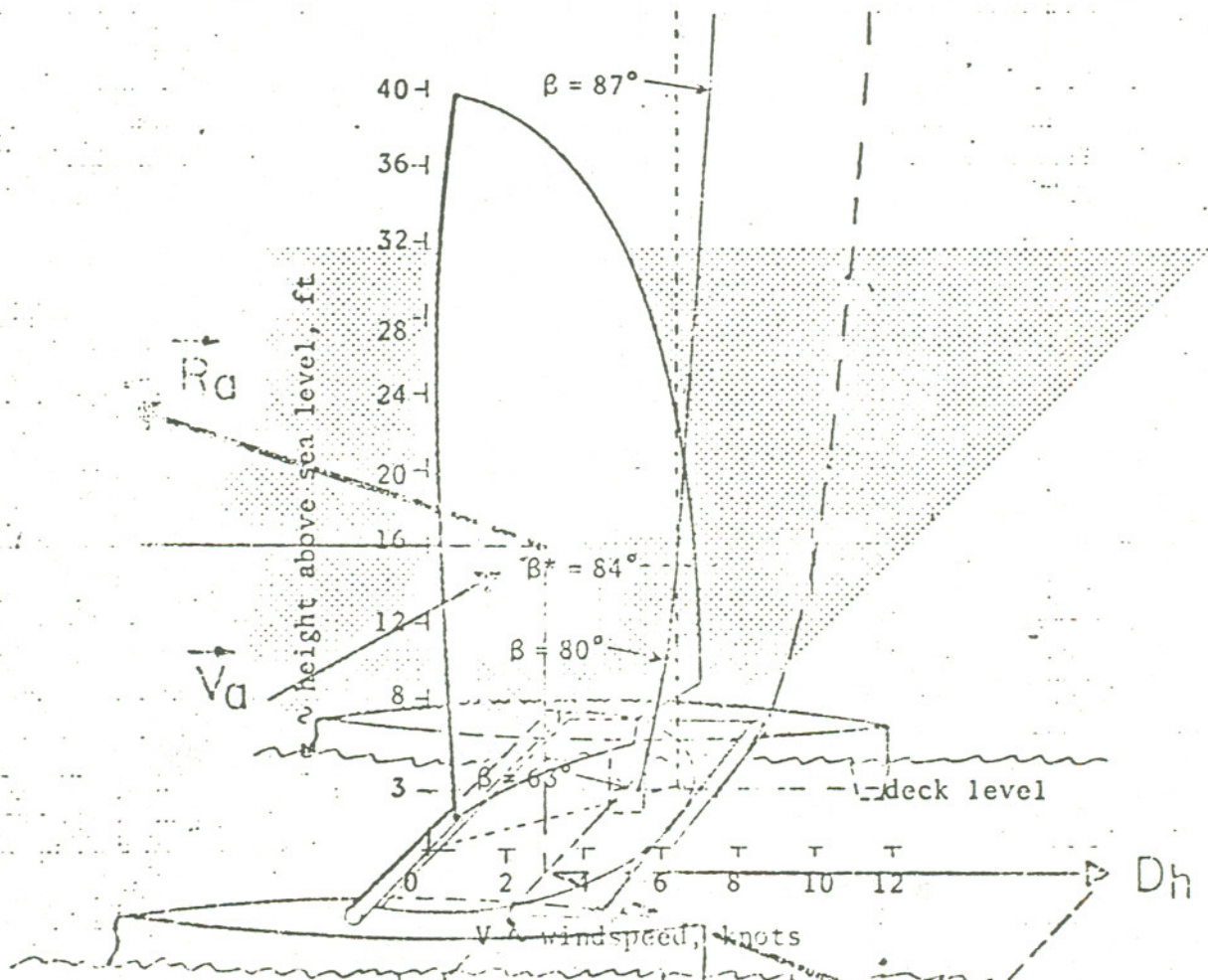——— apparent wind profile $V_a(z)$; (Table 3)

------ straightline profile [1]

Figure 12. Effects of the Natural Wind Profile on the Vehicle Apparent Wind Profile Tacking Downwind.
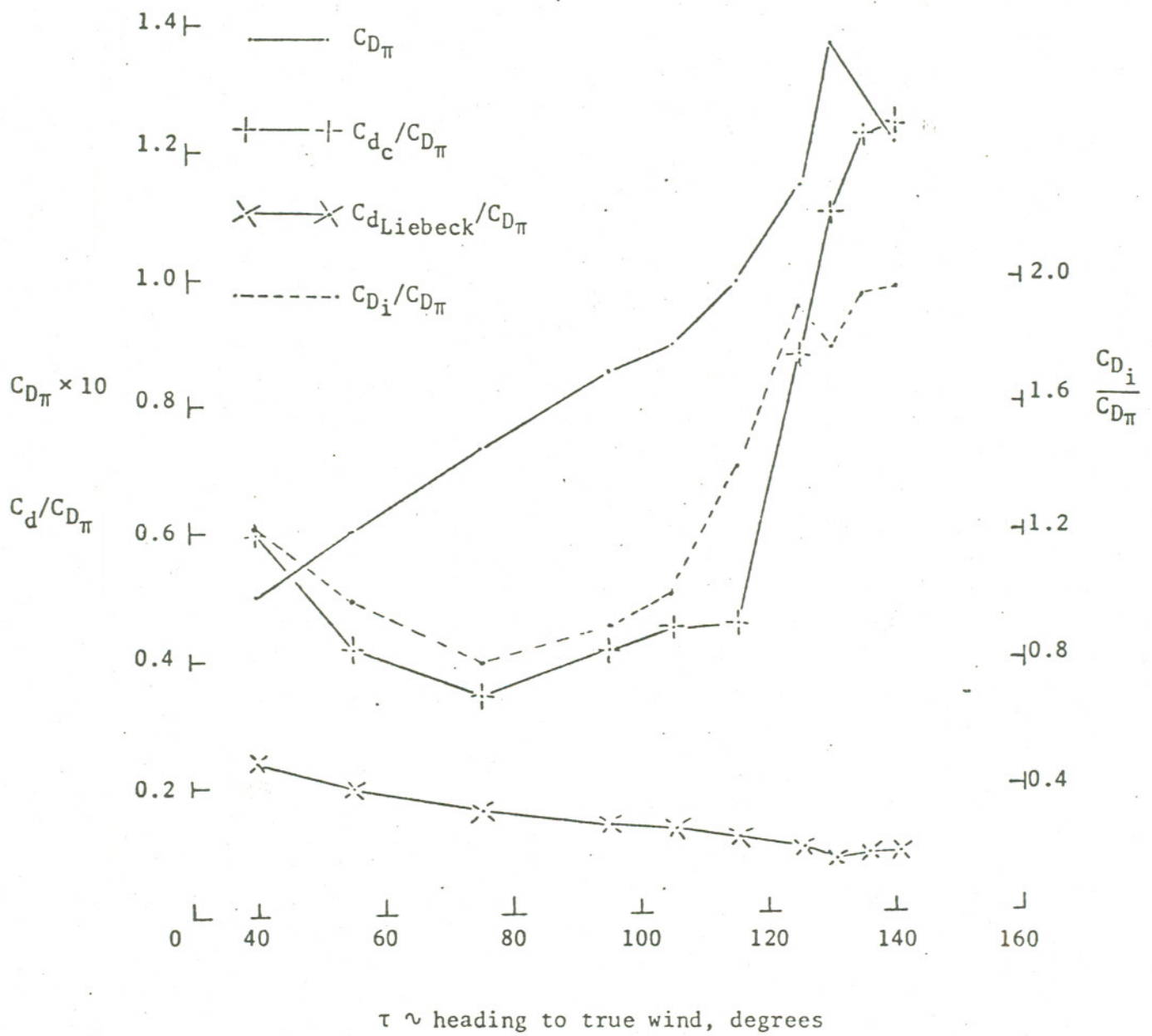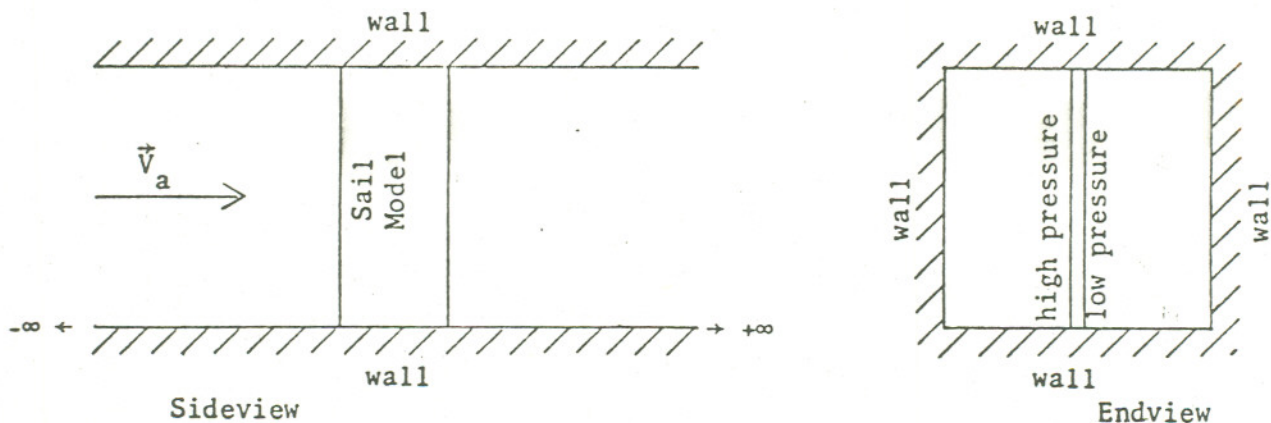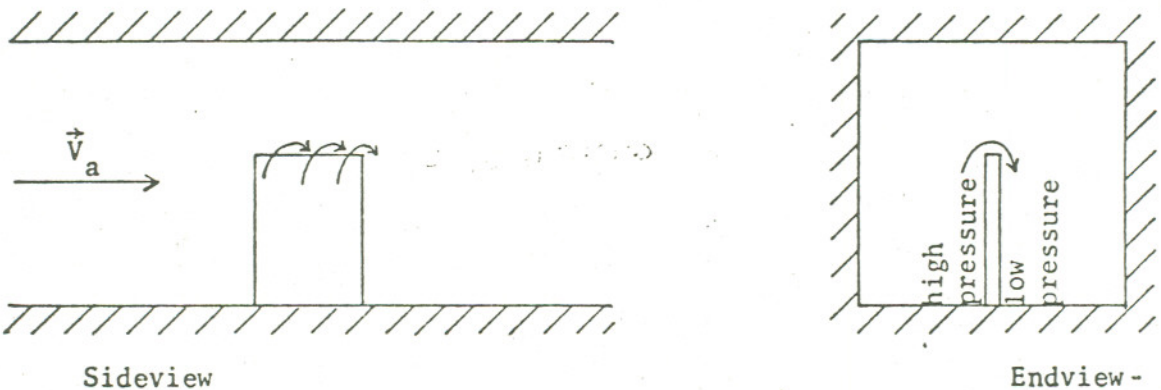
Figure 13. Variation of the Parasite Drag Coefficient with Heading to the True Wind (boat of Table 1).

(a) Two-Dimensional Flow About Sail Model
     in Wind Tunnel

(b) "Leakage" Around Tip in Three-Dimensional
     Flow

(c) "Leakage" Around Tip with Endplate (three-
     dimensional flow)

Figure 14.   A Qualitative Comparison of Two and Three-Dimensional
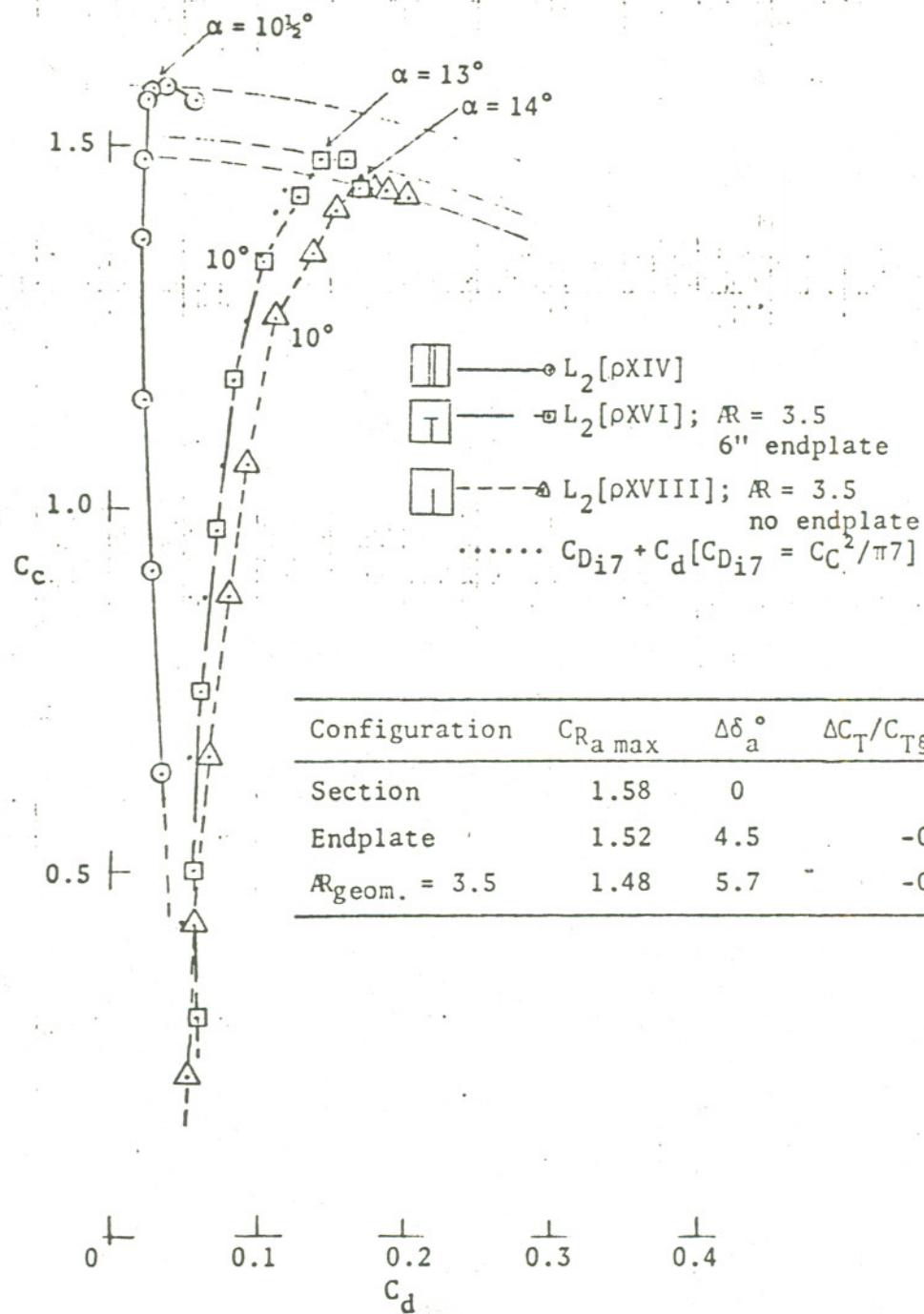   Flow About Sail Models.

The plot shows C_C versus C_d with data points labeled $\alpha = 10\frac{1}{2}°$, $\alpha = 13°$, $\alpha = 14°$, and $10°$, $10°$.

Legend:
- $L_2[\rho XIV]$
- $L_2[\rho XVI]$; $\mathcal{R} = 3.5$, 6" endplate
- $L_2[\rho XVIII]$; $\mathcal{R} = 3.5$, no endplate
- $\cdots\cdots\; C_{D_{i7}} + C_d\,[C_{D_{i7}} = C_C^2/\pi 7]$

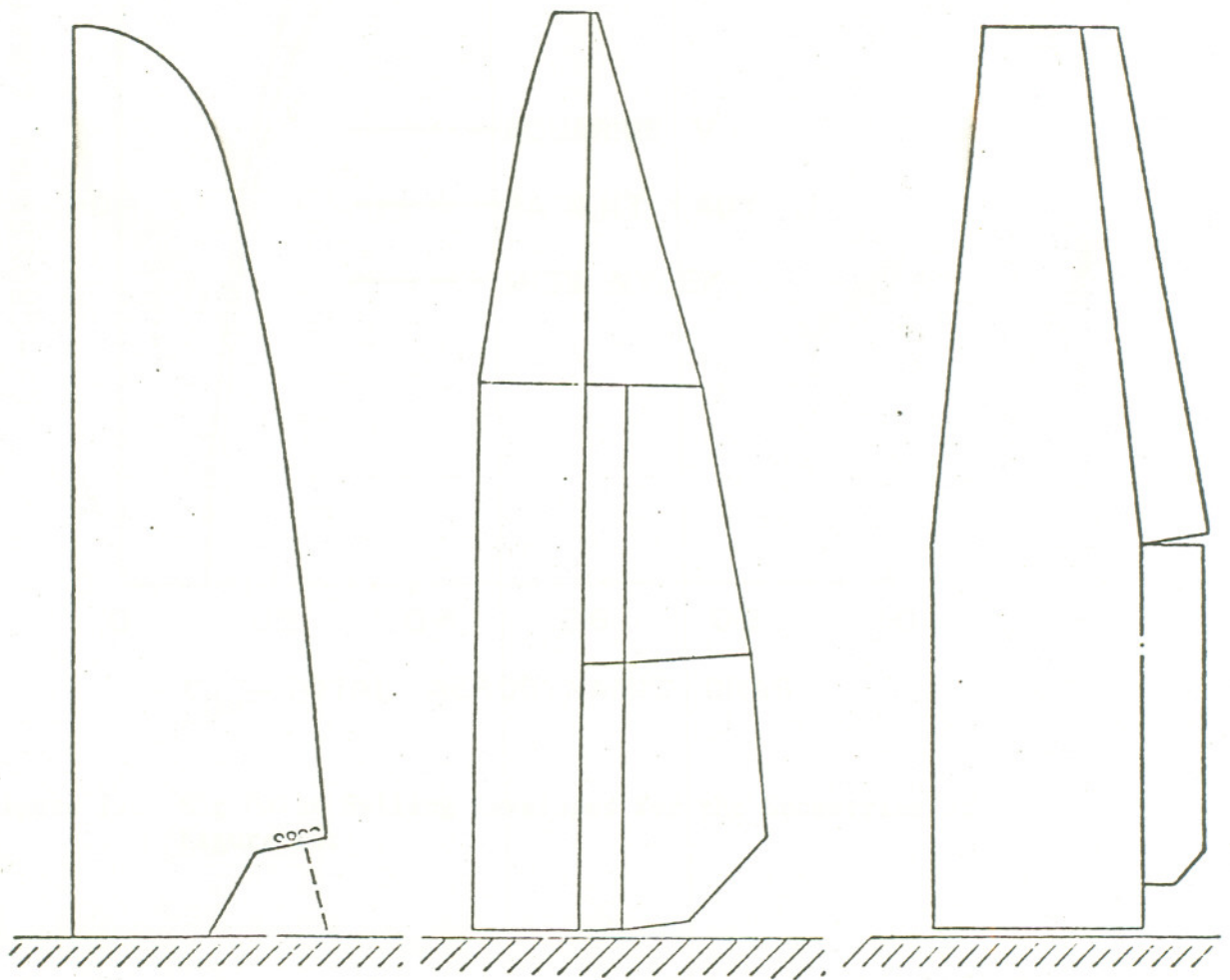| Configuration	$C_{R_a\,max}$	$\Delta\delta_a°$	$\Delta C_T/C_{T\S}]_{\tau=135°}$
Section	1.58	0	0
Endplate	1.52	4.5	−0.08
$\mathcal{R}_{geom.} = 3.5$	1.48	5.7	−0.12

Figure 15. A Quantitative Comparison of the Three-Dimensional Flow Effects (configurations) of Figure 14).

	AQUARIUS V	PATIENT LADY II	MISS NYLEX
Mast Ht.	36.5	36.0	36.0
$\mathbb{R}$	4.4	4.3	4.3
$\mathbb{R}_{eff}$	6.1	6.0	5.9
Area	300	300	300
Rig Wt.	98	200	210
Sailing Wt.	790	892	902

Figure 16. Comparative Rig Planform Geometry of Three Currently Competing
C-class Rigs.

Appendix 1

Effect of Hooked Leech on Performance of Boat of Table 2

We pointed out in Part 1 (pp. 6, 10) that moving the maximum camber too far aft results in a hooked leech configuration with resulting loss of sail performance due to greater flow separation. The center of effort also moves aft for such a configuration and the wind tunnel data [10] show that for this case the movement is from about 30% chord to about 55% chord for the NACA 0015/2 cases of Figure 6. If we put this section on the hulls of the boat of Figure 1 (Table 2) the effects of hooking the leech are two: i) the drag angle is increased so there will be a thrust loss at every value of sail force C_{R_a}; and ii) helm imbalance will result from the center of effort shift. Since the vehicle is assumed balanced with the maximum camber forward, the aft shift will be expected to produce weather helm and to load the rudders, thereby changing the hull drag distribution. Since the percent chord shift is nearly constant over the range of C_{R_a} considered, $[\overline{\Delta x}/c]$ was considered constant in this case and the yawing couple $(\dot= C_{R_a}(\tau)[\overline{\Delta x}/c])$ was carried through the computer program to provide the required rudder sideloading as a function of vehicle heading. The result is shown as Figure A-1. Note that only one camber is used, namely $7\frac{1}{2}\%$ (Figure 3). However, the results should be regarded as typical of the normal camber operating range.

The figure shows results which correspond qualitatively with experience. Maximum camber forward yields the best performance over

NACA 0015/2 data (Figure 6)

NACA 0015/2 hooked leech (Figure 6) including helm imbalance (weather helm)

hooked leech case with helm imbalance removed
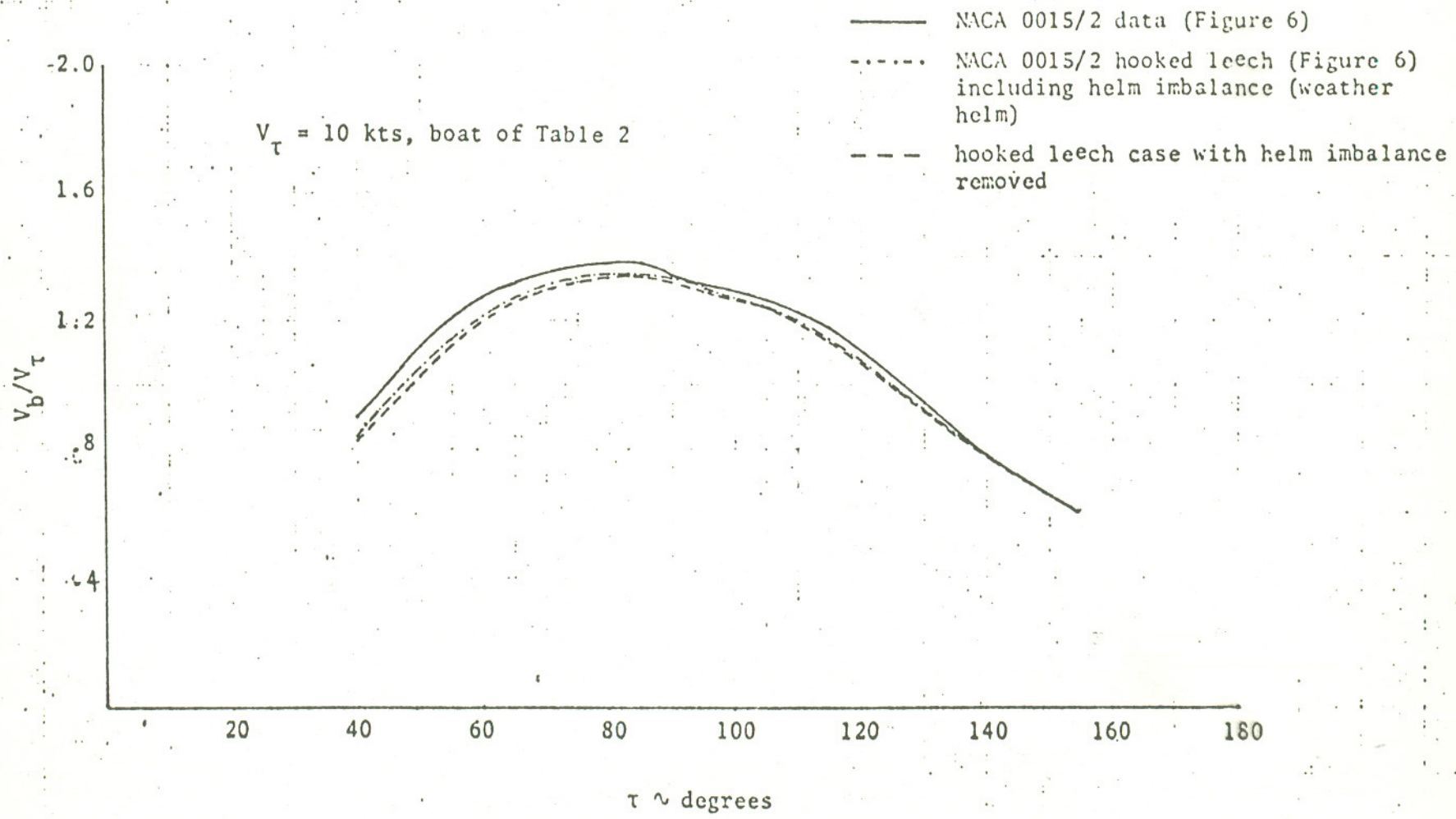
V_τ = 10 kts, boat of Table 2

V_b/V_τ

$\tau \sim$ degrees

Figure A-1. Hooked Leech Effect on Hulls of Table 2.